

# DIFFUSION OF MAGNETIC FIELD AND HEAT IN TURBULENT ASTROPHYSICAL FLUIDS AND REMOVAL OF MAGNETIC FLUX FROM TURBULENT CLOUDS

R. SANTOS-LIMA<sup>1</sup>, A. LAZARIAN<sup>2</sup>, E. M. DE GOUVEIA DAL PINO<sup>1</sup>, J. CHO<sup>2,3</sup>

*Draft version April 28, 2019*

## ABSTRACT

The diffusion of astrophysical magnetic fields in conducting fluids in the presence of turbulence depends on whether magnetic fields can change their topology or reconnect in highly conducting media. Recent progress in understanding fast magnetic reconnection in the presence of turbulence is reassuring that the magnetic field behavior in the computer simulations and turbulent astrophysical environments is similar, as far as the magnetic reconnection is concerned. This makes it meaningful to perform MHD simulations of turbulent flows in order to understand the diffusion of magnetic field in astrophysical environments. Our study of heat transfer in compressible fluids provides high rates of turbulent advection of heat and extends earlier relevant study. At the same time, our studies of magnetic field diffusion in turbulent medium reveal interesting new phenomena. First of all, our 3D MHD simulations initiated with anti-correlating magnetic field and gaseous density exhibit at later times a de-correlation of the magnetic field and density, which corresponds well to the observations of the interstellar media. Contrary to the earlier claims on the role of the ambipolar diffusion for de-correlating magnetic field and density, we get the effect with one fluid code, i.e. without invoking ambipolar diffusion. In addition, in the presence of gravity and turbulence, our 3D simulations show the decrease of the flux-to-mass ratio as density at the center of gravitational potential increases. We observe this effect both in the situations when we start with equilibrium distributions of gas and magnetic field and when we follow the evolution of collapsing dynamically unstable configurations. Thus the process of turbulent magnetic field removal should be applicable both to quasistatic subcritical molecular clouds and cores and violently collapsing supercritical entities. The increase of the gravitational potential as well as the magnetization of the gas increases the segregation of the mass and magnetic flux in the saturated final state of the simulations, supporting the notion that turbulent diffusivity relaxes the magnetic field + gas system in the gravitational field to its minimal energy state. This effect is expected to play an important role on star formation, from its initial stages of concentrating of interstellar gas to the final stages of the accretion to the forming protostar.

*Subject headings:* diffusion — ISM: magnetic fields — MHD — turbulence

## 1. INTRODUCTION

Astrophysical flows are known to be turbulent and magnetized. The specific role played by MHD turbulence in different branches of Astrophysics is still highly debated, but it is generally regarded as important. In particular, for the ISM and star formation, the role of turbulence has been discussed in many reviews (see Elmegreen & Scalo 2004; McKee & Ostriker 2007). The opinion on the role of magnetic field in these environments vary from magnetic field being regarded as absolutely dominant in the processes (see Tassis & Mouschovias 2005; Galli et al. 2006) to moderately important, as in super-Alfvénic models of star formation (see Padoan et al. 2004).

The important question that frequently permeates these debates is the diffusion of the magnetic field in astrophysical fluids. The conductivity of most of the astrophysical fluids is high enough to make the Ohmic diffusion negligible on the scales involved, which means that the “frozen-in” approximation is a good one for many as-

trophysical environments. However, without considering diffusive mechanisms that can violate the flux freezing, one faces problems attempting to explain many observational facts. For example, simple estimates show that if all the magnetic flux is brought together with the material that collapses to form a star in molecular clouds, then the magnetic field in a proto-star should be several orders of magnitude higher than the one observed in T-Tauri stars (the “magnetic flux problem”, see Galli et al. 2006 and references therein, for example).

To address the problem of the magnetic field diffusion both in the partially ionized ISM and in molecular clouds, researchers usually appeal to the ambipolar diffusion concept (see Mestel 1985; Shu 1983). The idea of the ambipolar diffusion is very simple and may be easily exemplified in the case of gas collapsing to form a protostar. As the magnetic field is acting on charged particles only, it does not directly affect neutrals. Neutrals move under the gravitational pull but are scattered by collisions with ions and charged dust grains which are coupled with the magnetic field. The resulting flow dominated by the neutrals will be unable to drag the magnetic field lines and these will diffuse through the infalling matter. This process of ambipolar diffusion becomes faster as the ionization ratio decreases and therefore, becomes

<sup>1</sup> Astronomy Department, Universidade de São Paulo, Brazil

<sup>2</sup> Department of Astronomy, University of Wisconsin, Madison, WI 53706, USA

<sup>3</sup> Dept. of Astronomy and Space Science, Chungnam National Univ., Daejeon, Korea

more important in poorly ionized cloud cores.

Shu et al. (2006) have explored the accretion phase in low-mass star formation and concluded that there should exist an effective diffusivity about four orders of magnitude larger than Ohmic diffusivity in order for an efficient magnetic flux transport to occur. They have argued that ambipolar diffusion could work, but only under special circumstances like, for instance, considering specific dust grain sizes. In other words, there is still no consensus if ambipolar diffusion is really high enough to solve the magnetic flux transport problem in collapsing flows.

Does magnetic field remain absolutely frozen-in within highly ionized astrophysical fluids? The answer to this question affects the description of several other processes in the interstellar and intergalactic gas.

A process that can remove the constraints connected with magnetic field being frozen with the gas is magnetic reconnection. Magnetic reconnection was shown to allow heat transport with coefficients very similar to those of hydrodynamic turbulent diffusivity within a magnetized turbulent fluid (Cho et al. 2003). However, the fact that this process was shown to be present in numerically computed fluids does not prove that the process is also efficient for astrophysical flows. The catch here is that the reconnection in computational fluids is usually fast, as the corresponding Lundquist numbers  $S = LV_A/\eta$  (where  $L$  is the scale of the flow,  $V_A$  is the Alfvén velocity of the fluid,  $\eta$  is the resistivity) are small compared to the real values of  $S$  that characterize astrophysical flows. In the most robust scheme of laminar magnetic reconnection, the speed of reconnection, i.e. the speed with which magnetic field lines change their topology, scales as  $S^{-1/2}$ . If the computed reconnection rates were slow, then one should not believe in any results of magnetized numerical simulations, including those in Cho et al. (2003).

Fortunately, it has been recently shown numerically (see Kowal et al. 2009) that 3D magnetic reconnection in turbulent fluid follows the predictions of the reconnection model of Lazarian & Vishniac (1999) and therefore, is fast<sup>4</sup>. Motivated by this fact, here we perform simulations aiming to gain understanding of the diffusion of magnetic field induced by turbulence. We also perform simulations including turbulent heat diffusion, which allow us to compare our results with those in the literature.

It is well known that turbulence can enhance diffusive processes, bringing the diffusive rates to values dependent on the dynamic properties of the flow rather than on the microscopic physics. Cho et al. (2003) found that the transport properties of turbulent flows in the presence of magnetic fields are very similar to those of usual hydrodynamic turbulence, and that the magnetic fields do not suppress severely the diffusion in its perpendicular direction. What are the laws that govern *magnetic field diffusion* in turbulent magnetized fluids? Could those

<sup>4</sup> There is no contradiction in our claiming that we may worry about numerical reconnection happening in MHD simulations of turbulent flows and at the same time, test the model with MHD simulations. In the specially designed numerical tests the parameters of reconnection are well controlled and the corresponding  $S$  can be made high enough, so that even with the present day numerical simulations the reconnection occurs at rates which are less than  $V_A$ . Moreover, the results are compared with analytical predictions.

affect our understanding of basic interstellar and star formation processes? These are the questions that we address in the paper.

In this study, we try to understand the diffusion of magnetic field in a couple of idealized models in the presence of turbulence. We explore setups both with and without gravity and compare the diffusion of magnetic field with that of a passive scalar. In the context of star formation an important issue that we will address is an alternative way of decreasing the magnetic flux-to-mass ratio without appealing to ambipolar diffusion. The turbulence in our simulation is externally driven, but since turbulence in astrophysics is really ubiquitous, our results should be widely applicable.

The paper is organized as follows: In §2 we draw the theoretical grounds about fast magnetic reconnection. In §3, we describe the numerical code employed. In §4, we present our results about diffusion of passive scalars. In §5 we present the results concerning the diffusion of magnetic field in a setup without external forces. In §6 we present the results of our experiments of diffusion of magnetic field in the presence of a gravitational field. In §7 we discuss our results and compare with previous works. In §8 we discuss the accomplishments and limitations of our present study. In §9, we discuss our findings in the context of strong turbulence theory, and finally in §10 we summarize our conclusions.

## 2. FAST MAGNETIC RECONNECTION IN THE PRESENCE OF TURBULENCE AND MAGNETIC DIFFUSION DUE TO RECONNECTION

The dynamical response of magnetic fields in turbulent fluids, as we discussed above, depends on the the ability of magnetic fields to change their topology via reconnection. We know from observations that magnetic field reconnection may be both fast and slow. Indeed, a slow phase of reconnection is necessary in order to explain the accumulation of free energy associated with magnetic flux that precedes eruptive flares in magnetized coronae. Thus it is important to identify the conditions for the reconnection to be fast. Different mechanisms prescribe different conditions for this to happen.

The problem of magnetic reconnection is most frequently discussed in terms of solar flares. In fact, this is a fundamental process underlying the dynamics of magnetized fluids in general. If the magnetic field lines in a turbulent fluid does not easily reconnect, the properties of the fluid should be dominated by intersecting magnetic flux tubes which are unable to pass through each other. Such fluids cannot be simulated in a computer as magnetic flux tubes readily reconnect in the numerical simulations which are currently very diffusive compared to the actual astrophysical flows.

The famous Sweet-Parker model of reconnection (Sweet 1958; Parker 1958) (see Figure 1, upper panel) produces reconnection rates which are smaller than the Alfvén velocity by a square root of the Lundquist number, i.e. by  $S^{-1/2} \equiv (LV_A/\eta)^{-1/2}$ , where  $L$  in this case is the length of the current sheet. Thus this scheme produces reconnection at a rate which is negligible for most of astrophysical circumstances. If the Sweet-Parker were proven to be the only possible model of reconnection, it would have been possible to show that MHD numerical simulations do not have anything to do with real astro-

physical fluids. Fortunately, faster schemes of reconnection are available.

The first model of fast reconnection proposed by Petschek (1964) assumed that magnetic fluxes get into contact not along the astrophysically large scales of  $L$ , but instead over a scale comparable to the resistive thickness  $\delta$ , forming a distinct X-point, where magnetic field lines of the interacting fluxes converge at a sharp point to the reconnection spot. The stability of such a reconnection geometry in astrophysical situations is an open issue. At least for uniform resistivity, this configuration was proven to be unstable and to revert to a Sweet-Parker configuration (Biskamp 1986; Uzdensky & Kulsrud 2000).

Recent years have been marked by the progress in understanding some of the key processes of reconnection in astrophysical plasmas. In particular, a substantial progress has been obtained by considering reconnection in the presence of the Hall-effect (Shay et al. 1998, 2004). The condition for which the Hall-MHD term becomes important for the reconnection is that the ion skin depth  $\delta_{ion}$  becomes comparable with the Sweet-Parker diffusion scale  $\delta_{SP}$ . The ion skin depth is a microscopic characteristic and it can be viewed as the gyroradius of an ion moving at the Alfvén speed, i.e.  $\delta_{ion} = V_A/\omega_{ci}$ , where  $\omega_{ci}$  is the cyclotron frequency of an ion. For the parameters of the interstellar medium (see Table 1 in Draine & Lazarian 1998), the reconnection is collisional (see further discussion in Yamada et al. 2006).

To deal with both collisional and collisionless plasma Lazarian & Vishniac (1999, henceforth LV99) proposed a model of fast reconnection in the presence of weak turbulence when magnetic field back-reaction is extremely important. We stress that the LV99 model does not assume that the magnetic field can be easily bent by fluid motions, which is a usual assumption to “justify” and incorrect concept of turbulent diffusivity in the mean field dynamo.

The middle and bottom panels of Figure 1 illustrate the key components of LV99 model<sup>5</sup>. The reconnection events happen on small scales  $\lambda_{||}$  where magnetic field lines get into contact. As the number of independent reconnection events that take place simultaneously is  $L/\lambda_{||} \gg 1$  the resulting reconnection speed is not limited by the speed of individual events on the scale  $\lambda_{||}$ . Instead, the constraint on the reconnection speed comes from the thickness of the outflow reconnection region  $\Delta$ , which is determined by the magnetic field wandering in a turbulent fluid. The model is intrinsically three dimensional<sup>6</sup> as both field wandering and simultaneous entry of many independent field patches, as shown in Figure 1, are 3D effects. The magnetic reconnection speed becomes comparable with  $V_A$  when the scale of magnetic field wandering  $\Delta$  becomes comparable with  $L$ .<sup>7</sup>

<sup>5</sup> The cartoon in Figure 1 is an idealization of the reconnection process as the actual reconnection region also includes reconnected open loops of magnetic field moving oppositely to each other. Nevertheless, the cartoon properly reflects the role of the 3-dimensionality of the reconnection process, the importance of small-scale reconnection events, and the increase of the outflow region compared to the Sweet-Parker scheme.

<sup>6</sup> Bidimensional numerical simulations of turbulent reconnection in Kulpa-Dybel et al. (2009) show that the reconnection is not fast in this case.

<sup>7</sup> Another process that is determined by magnetic field wander-

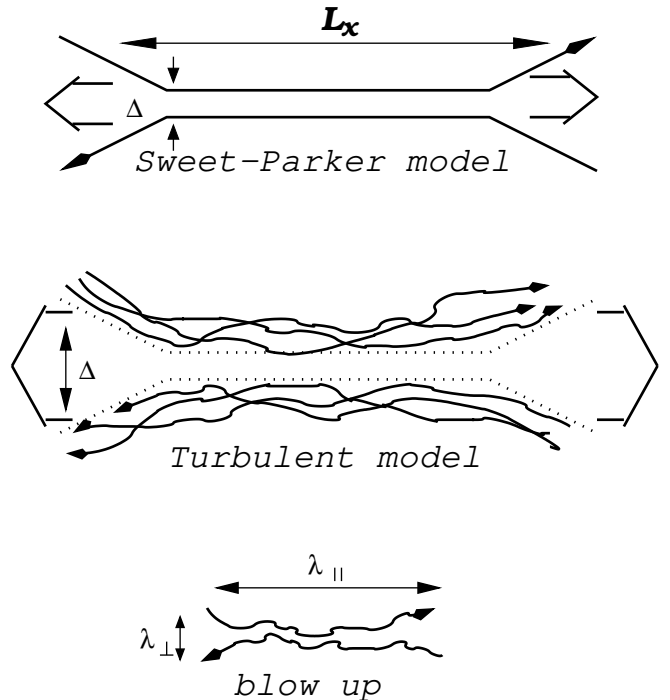


FIG. 1.— *Upper plot*: Sweet-Parker model of reconnection. The outflow is limited by a thin slot  $\Delta$ , which is determined by Ohmic diffusivity. The other scale is an astrophysical scale  $L \gg \Delta$ . *Middle plot*: Reconnection of weakly stochastic magnetic field according to LV99. The model that accounts for the stochasticity of magnetic field lines, which depends on field line stochasticity. *Low plot*: An individual small scale reconnection region. The reconnection over small patches of magnetic field determines the local reconnection rate. The global reconnection rate is substantially larger as many independent patches come together. From Lazarian et al. (2004).

For a quantitative description of the reconnection, one should adopt a model of MHD turbulence (see Iroshnikov 1963; Kraichnan 1965; Dobrowolny et al. 1980; Shebalin et al. 1983; Montgomery & Turner 1981; Higdon 1984). The most important for magnetic field wandering is the Alfvénic component. Adopting the Goldreich & Sridhar (1995, henceforth GS95) scaling of the Alfvénic component of MHD turbulence extended to include the case of weak turbulence, LV99 predicted that the reconnection speed in a weakly turbulent magnetic field is

$$V_R = V_A(l/L)^{1/2}(v_l/V_A)^2 \quad (1)$$

where the level of turbulence is parameterized by the injection velocity; the combination  $V_A(v_l/V_A)^2$  is the velocity of the largest strong turbulence eddies  $V_{strong}$ , i.e. the velocity at the scale at which the Alfvénic turbulence transfers from the weak to the strong regimes. Thus Eq. (1) can also be rewritten as  $V_R = V_{strong}(l/L)^{1/2}$ .  $v_l < V_A$  and the turbulence injection scale  $l$ .

The scaling predictions given by Eq. (1) have been tested successfully by 3D MHD numerical simulations in Kowal et al. (2009). This stimulates us to adopt the

ing is the diffusion of energetic particles perpendicular to the mean magnetic field. Indeed, the coefficient of diffusion perpendicular to the magnetic field in the Milky Way is just an order unity less than the coefficient of diffusion parallel to the magnetic field (see Giacalone & Jokipii 1999 and ref. therein).

LV99 model as a starting point for our discussion of magnetic reconnection.

How can  $\lambda_{\parallel}$  be determined? In LV99 model, as many as  $L^2/\lambda_{\perp}\lambda_{\parallel}$  localized reconnection events take place, each of which reconnects the flux at the rate  $V_{rec,local}/\lambda_{\perp}$ , where  $V_{rec,local}$  is the velocity of local reconnection events at the scale  $\lambda_{\parallel}$ . The individual reconnection events contribute to the global reconnection rate, which in 3D becomes a factor of  $L/\lambda_{\parallel}$  larger, i.e.

$$V_{rec,global} \approx L/\lambda_{\parallel}V_{rec,local}. \quad (2)$$

The local reconnection speed, conservatively assuming that the local events are happening at the Sweet-Parker rate, can be easily obtained by identifying the local resistive region  $\delta_{SP}$  with  $\lambda_{\perp}$  and using the relations between  $\lambda_{\parallel}$  and  $\lambda_{\perp}$  that follow from the MHD turbulence model. The corresponding calculations in LV99 provided the local reconnection rate  $v_l S^{-1/4}$ . Substituting this local reconnection rate in Eq. (2) one estimates the global reconnection speed, *if this speed were limited by Ohmic resistivity*, which is larger than  $V_A$  by a factor  $S^{1/4}$ . As a result, one has to conclude that the reconnection does not depend on resistivity.

The LV99 model is applicable to situations when plasma effects are included, e.g. the Hall-MHD effect, which increases effective resistivities for local reconnection events. While the latter point is difficult to test directly with existing plasma codes, e.g. with PIC codes, due to the necessity of simulating both plasma microphysics effects as well as macrophysical effects of magnetic turbulence, Kowal et al. (2009) simulated the action of plasma effects by parameterizing them via anomalous resistivities. The values of such resistivities are a steep function of the separation between oppositely directed magnetic field lines, which also determines the current separating magnetic fluxes. With anomalous resistivities, the structure of the fractal current sheet of the turbulent reconnection changed substantially, but no significant changes of the reconnection rate was reported, which agrees well with the theoretical expectations of LV99. Within the model the explanation of this stems from the fact that the reconnection is already fast (i.e. independent of resistivity) even when small scale reconnection events are mediated by the Ohmic resistivity, while the bottleneck for the reconnection process is provided by magnetic field wandering. Thus the increase of the local reconnection rate does not increase the global reconnection speed.

In this work, we address the problems relevant to the reconnection in a partially ionized, weakly turbulent gas. The corresponding model of reconnection was proposed in Lazarian et al. (2004, henceforth LVC04). The extensive calculations summarized in Table 1 in LVC04 show that the reconnection for realistic circumstances varies from  $0.1V_A$  to  $0.03V_A$ , i.e. is also fast, which should enable fast diffusion arising from turbulent motions.

The fact that magnetic fields reconnect fast in turbulent fluids ensures that the large scale dynamics that we can reproduce well with numerical codes is not compromised by the difference in reconnection processes in the computer and in astrophysical flows. This motivates our present study in which we investigate diffusion processes in turbulent magnetized fluids via 3D simulations. We

feel that the issue of the dimension of the simulations is crucial for the turbulence dynamics and therefore for our final results.

Visualization of turbulent diffusion of heat or any passive scalar field is easy within the GS95 model, which can be interpreted as a model of Kolmogorov cascade perpendicular to the local direction of the magnetic field (LV99 and more discussion in §8). The corresponding eddies are expected to advect heat similarly to the case of the hydrodynamic heat advection. The corresponding visualization of the magnetic field diffusion is more involved. Every time as magnetic field lines intersect each other, they change their configuration draining free energy from the system. In the presence of self-gravity this may mean the escape of magnetic field, which is a “light fluid” from the self-gravitating gaseous “heavy fluid”. Naturally, if the turbulence gets strong the system gets unbound and then the mixing of magnetic field and gas, rather than their segregation is expected. In what follows we test these ideas numerically.

### 3. MHD EQUATIONS AND THE NUMERICAL CODE

The systems studied numerically in this work are described by the resistive MHD equations, assuming an isothermal equation of state:

$$\frac{\partial \rho}{\partial t} + \nabla \cdot (\rho \mathbf{u}) = 0 \quad (3)$$

$$\rho \left( \frac{\partial}{\partial t} + \mathbf{u} \cdot \nabla \right) \mathbf{u} = -c_s^2 \nabla \rho + (\nabla \times \mathbf{B}) \times \mathbf{B} - \rho \nabla \Psi + \mathbf{f} \quad (4)$$

$$\frac{\partial \mathbf{B}}{\partial t} = \nabla \times (\mathbf{u} \times \mathbf{B}) + \eta_{Ohm} \nabla^2 \mathbf{B} \quad (5)$$

plus the divergenceless condition for the magnetic field  $\nabla \cdot \mathbf{B} = 0$ . The spatial coordinates are given in units of a typical length  $L_*$ . The density  $\rho$  is normalized by a reference density  $\rho_*$ , and the velocity field  $\mathbf{u}$  by a reference velocity  $U_*$ . The constant sound speed  $c_s$  is also given in units of  $U_*$ , and the magnetic field  $\mathbf{B}$  is measured in units of  $U_* \sqrt{4\pi \rho_*}$ . The uniform Ohmic resistivity  $\eta_{Ohm}$  is given in units of  $U_* L_*$ . In our numerical calculations we will use both non-zero and zero values of  $\eta_{Ohm}$ . In the latter case, the calculations will include only numerical resistivity. Time  $t$  is measured in units of  $L_*/U_*$ . The external gravitational potential  $\Psi$  is given in units of  $U_*^2$ . The source term  $\mathbf{f}$  is a random force term responsible for injection of turbulence.

The above equations are solved inside a three-dimensional box with periodic boundary conditions. We use a shock-capturing Godunov-type scheme with an HLL solver (see, for example, Kowal et al. 2007; Falceta-Gonçalves et al. 2008). Time integration is performed with the Runge-Kutta method of second order. Unless we say explicitly the opposite, we assume  $\eta_{Ohm} = 0$ .

We employ an isotropic, non-helical, solenoidal, delta correlated in time forcing  $\mathbf{f}$ . This forcing acts in a thin shell around the wave number  $k_f = 2.5(2\pi/L)$ , that is, the scale of turbulence injection  $l_{inj}$  is about 2.5 times smaller than the box size  $L$  (in all the simulations, we choose  $L = 1$  in code units). In most of the experiments, the *rms* velocity  $V_{rms}$  induced by turbulence in the box is close to unity (in code units).

Therefore, in these cases, the circulation time of the energy-carrying eddies (or the turbulent time-scale  $t_{turb}$ ) is  $t_{turb} \sim l_{inj}/v_{turb} \sim (L/2.5)/V_{rms} \approx 0.4$  units of time in code units.

We note that for our present purposes we use an one-fluid approximation, which does not include ambipolar diffusion. This choice is appropriate for approximating a fully ionized gas as well as for the description of the fluid dynamics on scales larger than the scale of ambipolar diffusion.

#### 4. TEST CASE: TURBULENT ADVECTION OF HEAT

We start by studying the three-dimensional transport properties of MHD turbulence. Our setup is identical to that adopted in Cho et al. (2003). Our goal is to provide simulations with higher numerical resolution (the resolution employed in Cho et al. 2003 is mostly  $192^3$ ) and for a larger parameter space. In the present work, we study how compressibility and magnetization affect the results. We note that at the time when the results in Cho et al. (2003) were obtained the issues of reconnection in turbulent media were more speculative. Thus, after numerical testing of the model of reconnection in LV99 by Kowal et al. (2009), we feel it is appropriate to revisit that domain.

Besides the ideal MHD set of equations, we also evolve four independent fields of passive scalars  $\Phi_\alpha(\mathbf{x})$  ( $\alpha = 1, 2, 3, 4$ ) by the continuity equation:

$$\frac{\partial \Phi_\alpha}{\partial t} + \nabla \cdot (\Phi_\alpha \mathbf{u}) = 0 \quad (6)$$

These passive scalar fields can trace, for example, the volume concentration of some physical property of the gas, like metallicity or heat<sup>8</sup>, as long as the time-scale associated with the molecular (microscopic) diffusion is larger than the typical dynamical time-scale of the flow. In our simulations this is ensured by fluids being turbulent<sup>9</sup>.

These passive scalar fields are assumed to have initial spherical symmetry with a gaussian radial profile:

$$\Phi_\alpha(\mathbf{x}, t = 0) = \exp \left\{ 3(\mathbf{x} - \mathbf{x}_0)^2 / 2\sigma_0^2 \right\} \quad (7)$$

where  $\mathbf{x}_0$  is the center of the box and, as in Cho et al. (2003), we choose the initial dispersion  $\sigma_0 = L\sqrt{3}/16\sqrt{2}$  ( $\approx 19$  grid cells, for the resolution employed of  $256^3$ ), to ensure that the characteristic width  $\sigma_0$  is inside the inertial range of the turbulence. This initial distribution of  $\Phi_\alpha$  is a natural choice to study its diffusion. If we had, for instance, a microscopic diffusion coefficient  $\kappa$ , the gaussian shape of the distribution would remain unaltered, with the dispersion increasing linearly in time at a rate  $\kappa$ .

The initial magnetic field  $\mathbf{B}_0$  is uniform and parallel to the  $x$ -direction, and the initial density field is also

<sup>8</sup> It may appear that there is some contradiction here between the assumption of an isothermal equation of state (which implies instantaneous heat diffusion) and the adoption of a variable scalar field to describe heat. However, if we had employed an adiabatic equation of state, the results below would not change sensitively, as long as turbulent transport of heating is concerned (e.g., Cho et al. 2003).

<sup>9</sup> As soon as the molecular diffusivity rate  $L^2/\eta$  gets larger than the rates associated with the flow, i.e.  $V/L$ , the corresponding Reynolds number  $Re = VL/\eta$  gets less than unity and turbulence decays at the scale  $L$ .

uniform with  $\rho = 1$ . The passive scalar fields are injected after the turbulence is fully developed. The first scalar-field  $\Phi_1$  is injected at  $t = 3$  (approximately 6 turn-over times), and the other fields ( $\alpha = 2, 3, 4$ ) at each time step after.

Table 1 shows the set of parameters studied. The magnetic field is given in terms of the initial Alfvén speed. Turbulence is injected with the same power  $\epsilon = 1$  in all the models. These runs cover four combinations of regimes of sonic and Alfvénic mach numbers ( $M_s$  and  $M_A$ , respectively). The quantities shown in Table 1 ( $M_s$ ,  $M_A$ ,  $V_{rms}$ ,  $B_{rms}$ ) are averages taken over the time after the injection of the first passive field (these time averages are over the available computed cubic domains taken at every 0.25 time step). The standard deviation of these averages are shown within parentheses. For each data cube, the Mach numbers correspond to the average of the local values computed over the entire box. The resolution employed in all the simulations is  $256^3$ .

#### 4.1. Results

Compressibility can change the properties of flows substantially. For instance, high Mach number turbulence is known to create regions of enhanced density which will coexist with the expanses of low density. At the same time, one should expect to see similarity between the properties of fluid in low-Mach number flows and incompressible flows.

We first consider a case of heat transport, which can be considered as a test case, as we can compare our results with the earlier heat transport simulations in Cho et al. (2003). This is the case where the back-reaction can be ignored and we can use a passive scalar diffusion to represent the diffusion of heat.

Let us relate the evolution of the dispersion  $\sigma$  with the turbulent diffusion coefficient  $\eta_{turb}$ , that is, the coefficient that gives the rate at which the passive scalar field diffuses in scales larger than the turbulent scale. The dispersion  $\sigma$  is calculated through the definition:  $\sigma^2 = \frac{\int (\mathbf{x} - \bar{\mathbf{x}})^2 \Phi(\mathbf{x}) d^3x}{\int \Phi(\mathbf{x}) d^3x}$ , where  $\bar{\mathbf{x}} = \frac{\int \mathbf{x} \Phi(\mathbf{x}) d^3x}{\int \Phi(\mathbf{x}) d^3x}$ . If  $\lambda$  is the *rms* distance between two fluid elements being advected, for  $\lambda$  higher than the injection scale of the turbulence  $l_{inj}$ , its evolution is related to  $\eta_{turb}$  by  $\delta\lambda^2 \sim \eta_{turb}\delta t$ .

Considering ordinary hydrodynamic turbulence, we can write, for the *rms* distance  $l$  between two fluid elements, within the inertial range:

$$\delta l^2 \sim v_l \delta t \quad (8)$$

where  $v_l$  is the velocity at scale  $l$ . From the assumption that both relations above should be valid at the scale  $l_{inj}$ , it must be true that  $\eta_{turb} \sim l_{inj} v_{turb}$ , and we could define a constant  $C_{dyn}$  so that:

$$\eta_{turb} = C_{dyn} l_{inj} v_{turb} \quad (9)$$

Now, one wonder if  $C_{dyn}$  is reduced by the magnetic field in magnetized turbulence (due to suppression of turbulent mixture).  $C_{dyn}$  is related to the constant of proportionality in equation (8). Again, let  $l$  be the distance between two fluid elements initially separated by a distance  $l_0$  within the inertial range in ordinary hydrodynamic turbulence. Repeating equation (8) and using the

TABLE 1  
SIMULATIONS OF THE TURBULENT DIFFUSION OF PASSIVE SCALAR FIELDS

Model	$c_s$	$B_0$	$M_s$	$M_A$	$V_{rms}$	$B_{rms}$	$C_*$	$C_*/V_{rms}$	Resolution
A1	3.0	0.1	0.25(0.00)	2.41(0.06)	0.75(0.01)	0.51(0.01)	0.4	$\approx 0.5$	$256^3$
A2	3.0	1.0	0.27(0.01)	0.78(0.03)	0.80(0.02)	1.23(0.01)	0.15	$\approx 0.2$	$256^3$
A3	0.1	0.1	7.53(0.13)	2.13(0.12)	0.75(0.01)	0.38(0.01)	0.4	$\approx 0.5$	$256^3$
A4	0.1	1.0	7.44(0.12)	0.55(0.01)	0.74(0.01)	1.14(0.01)	0.3	$\approx 0.4$	$256^3$

Kolmogorov's phenomenology,

$$\delta l \sim v_l \delta t \sim (\epsilon l)^{1/3} \delta t \quad (10)$$

where  $\epsilon$  is the power of injection (or dissipation) of the kinetic energy. Integrating the last expression,

$$l^{2/3} - l_0^{2/3} = C_R \epsilon^{1/3} (t - t_0) \quad (11)$$

where the dimensionless constant  $C_R$  is the Richardson constant (Richardson 1926; Lesieur 1990). Therefore,  $C_{dyn}$  is related to  $C_R$ .

Using the dispersion  $\sigma$  of our experiments as the  $rms$  distance  $l$  in the equation (11), and supposing that this equation remains valid in MHD turbulence,

$$\sigma^{2/3} - \sigma_0^{2/3} = C_* \epsilon^{1/3} (t - t_0) \quad (12)$$

where  $C_*$  has not necessarily the same value that  $C_R$ .

Figure 2 shows the evolution of  $(\sigma^{2/3} - \sigma_0^{2/3})$  for our models. We have made an offset of the values for each model in order to make the visualization easier. Table 1 lists the approximated values of  $C_*$  for the models, obtained from a linear fit of the data.

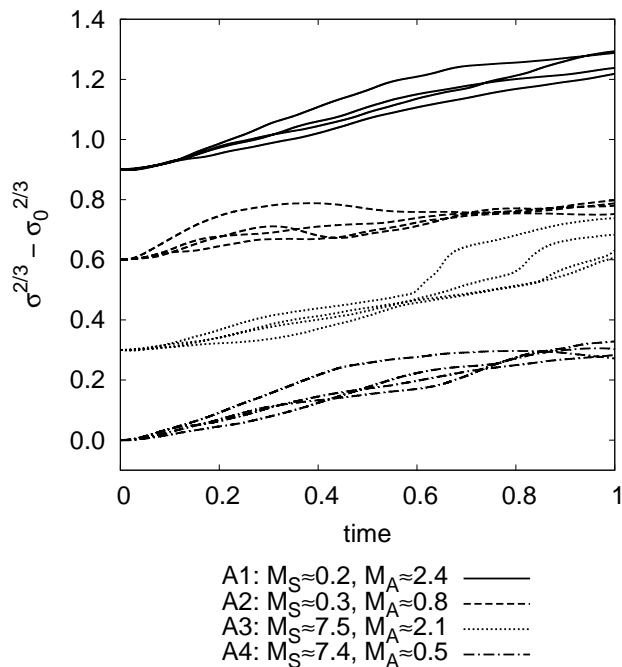


FIG. 2.— Evolution of  $\sigma^{2/3} - \sigma_0^{2/3}$  for different models, where  $\sigma^2 = \frac{\int (\mathbf{x} - \bar{\mathbf{x}})^2 \Phi(\mathbf{x}) d^3x}{\int \Phi(\mathbf{x}) d^3x}$  ( $\bar{\mathbf{x}} = \frac{\int \mathbf{x} \Phi(\mathbf{x}) d^3x}{\int \Phi(\mathbf{x}) d^3x}$ ). We have introduced an offset for the lines of each model in order to make the visualization clearer.

All in all, our results presented in Figure 2 are consistent with the scalings of diffusion showed in Cho et al. (2003). This indicates that the relation (12) continues approximately valid in the MHD case. The slopes do not seem to be very sensitive to  $M_s$ , but we can note a small difference for the trans-Alfvénic and super-Alfvénic cases, the constant  $C_*$  being a little higher in the super-Alfvénic cases. This finding is consistent with the prediction of changes of the diffusion efficiencies of Lazarian (2006). There it is shown that for higher magnetization, corresponding to an Alfvén Mach number  $M_A = V/V_A < 1$ , where  $V$  is the injection velocity and  $V_A$  is the Alfvén velocity, the turbulence at the large scales is weak, which produces weak mixing. In our parametrization this corresponds to the decrease of  $C_*$ , which is the case of A2 simulation. Interestingly enough, in the case of  $M_A < 1$  and  $M_s \gg 1$ , which is the case of A4 simulation, we see the increase of the  $C_*$ . The case of high Mach number turbulence is not covered by Lazarian (2006), but we expect that the concentration of gas in dense regions plays an important role for the effect. In regions of gas concentration the Alfvénic velocity and the corresponding  $M_A$  drops (see Burkhart et al. 2009). As a result, the mixing should be less constrained by the magnetic field as we see in the A4 model. Comparing cases A1 and A3 we observe that for super-Alfvénic turbulence and different Mach number  $M_s$  the diffusivity is rather similar.

Note that Cho et al. (2003) obtained the values of  $C_*/V_{rms} = 0.4$  ( $V_A = 0.1$  and  $M_s = 2.3$ ),  $0.3$  ( $V_A = 1$  and  $M_s = 2.3$ ),  $0.4$  ( $V_A = 1$  and  $M_s = 0.3$ ), and  $0.5$  (hydrodynamic case and  $M_s = 0.3$ ), which are consistent with our findings. In Cho et al. (2003),  $V_{rms} \approx 0.8$  in all the cases (to make a comparison we had to convert the time-scale to the present code units, i.e. 1 time step here =  $2\pi$  time steps there, see remark in §7.1). We conclude, that for a wide range of magnetizations and Mach numbers, turbulence is efficient in inducing turbulent diffusivity of heat.

## 5. TURBULENT MAGNETIC FIELD DIFFUSION IN THE ABSENCE OF GRAVITY

If turbulence can induce heat diffusion one can wonder whether it can induce the diffusion of magnetic field. Observations of different regions of the diffuse ISM compiled by Troland & Heiles (1986) indicate that magnetic fields and density are not straightforwardly correlated. These observations motivated Heitsch et al. (2004) to perform 2.5D numerical calculations in the presence of both ambipolar diffusion and turbulence. The results in Heitsch et al. (2004) also indicated de-correlation of magnetic field and density, but the constrained geometry of their simulations (where the magnetic field was assumed to be perpendicular to the plane of the 2D turbulence, so that there were no reconnection) weakened

the comparison of their considered idealized situation with the actual 3D effects in the 3D magnetized ISM. One may also wonder whether ambipolar diffusion is always required to de-correlate magnetic field and density or, on the contrary, a concept of “turbulent ambipolar diffusion” would be useful. To address these issues we performed 3D simulations of magnetic diffusion in the absence of ambipolar diffusion effects.

### 5.1. Numerical setup

The magnetic field is assumed to have initially only the component in the  $z$ -direction. The initial configuration of the magnetic and density fields are:

$$B_z(x, y) = B_0 + B_1 \cos\left(\frac{2\pi}{L}x\right) \cos\left(\frac{2\pi}{L}y\right) \quad (13)$$

$$\rho(x, y) = \rho_0 - \frac{1}{c_s^2} \left\{ B_0 B_1 \cos\left(\frac{2\pi}{L}x\right) \cos\left(\frac{2\pi}{L}y\right) + 0.5 [B_1 \cos\left(\frac{2\pi}{L}x\right) \cos\left(\frac{2\pi}{L}y\right)]^2 \right\} \quad (14)$$

where  $(x, y) = (0, 0)$  is the center of the  $x, y$ -plane. Boundary conditions are periodic.

This initial magnetic field configuration has an uniform component  $B_0$  plus an harmonic perturbation of amplitude  $B_1$ . The density field is distributed in such a way that the gas pressure, given by the isothermal equation of state  $p = c_s^2 \rho$ , equilibrates exactly the magnetic pressure, giving a magneto-hydrostatic solution. We choose the parameters  $B_1 = 0.3$ ,  $\rho_0 = 1$  and  $c_s = 1$  in all our simulations. Figure 3 illustrates these initial fields when  $B_0 = 1.0$ .

We should remark that the simulations presented in Heitsch et al. (2004) do not start at the equilibrium, like ours. There is no pressure term in their equation for the evolution of the momentum of the ions to counterbalance the magnetic pressure. In addition, in their work the ion-density field is kept constant in time and space.

Another difference between our setup and that in Heitsch et al. (2004) is that our parameter  $B_1$  is assumed to be the same for all the models studied, and not a fraction of  $B_0$ . Also, the amplitude of the perturbation of the homogeneous component of the density field is a free parameter in Heitsch et al. (2004), while here it is constrained by the imposed equilibrium between gas and magnetic pressures.

In addition, we introduce a passive scalar field  $\Phi$  initially identical to  $B_z$ . The parameters of our relevant simulations are presented in Table 2.

In these simulations we keep the random velocity approximately constant, i.e.  $V_{rms} \approx 0.8$  for all the models after one time step. Therefore, all these models are slightly subsonic.

### 5.2. Notation

Hereafter, the quantities within brackets with subscript “ $R = 0.25L$ ”:  $\langle \cdot \rangle_{R=0.25L}$ , or simply “0.25”:  $\langle \cdot \rangle_{0.25}$  will denote averages inside a cylinder with main-axis in the  $z$ -direction centered in the computational box, with radius  $R = 0.25L$ , while a subscript “ $z$ ”:  $\langle \cdot \rangle_z$  will denote an average over the  $z$  direction. An overbar means the average of some quantity inside the entire box.

### 5.3. Results

Figure 4 shows the time evolution of  $\langle B_z \rangle_{0.25} / \langle \rho \rangle_{0.25} - \bar{B}_z / \bar{\rho}$  and  $\langle \Phi \rangle_{0.25} / \langle \rho \rangle_{0.25} - \bar{\Phi} / \bar{\rho}$ . Both quantities have a similar behavior, and all models seem to achieve the characteristic average values ( $\bar{B}_z / \bar{\rho}$  and  $\bar{\Phi} / \bar{\rho}$ ) roughly at the same time.

Figure 5 shows the evolution of the amplitude of the mode that is identical to the initial harmonic perturbation of the magnetic field (i.e., the *rms* of the amplitude of the fourier modes  $(k_x, k_y) = (\pm 1, \pm 1)$ ), for  $\langle B_z \rangle_z$  (top left),  $\langle \Phi \rangle_z$  (top right),  $\langle B_z \rangle_z / \langle \rho \rangle_z$  (bottom left), and  $\langle \Phi \rangle_z / \langle \rho \rangle_z$  (bottom right). All the curves presented were smoothed in order to make the visualization clearer. We see that the decaying of the magnetic field occurs at a rate similar to that of the passive field. This mode decays nearly exponentially at roughly the same rate for most of the models. Only the model B1 ( $B_0 = 0.5$ ) exhibits a higher decay rate. This may be due to the large scale field reversals that are common in super-Alfvénic turbulence. Also, the decay rates for  $\langle B_z \rangle_z / \langle \rho \rangle_z$  and  $\langle \Phi \rangle_z / \langle \rho \rangle_z$  are similar for all the models except for the model B1, for which the rate is higher. Table 2 shows the fitted values (and the uncertainty) of  $\eta_{turb}$  for the curves corresponding to the evolution of the amplitude of the modes for  $\langle B_z \rangle_z$  and  $\langle \Phi \rangle_z$ . The fitted curve is  $\exp\{-k^2 \eta_{turb} t\}$ , where  $k^2 = k_x^2 + k_y^2 = 2$  is the module of the wave-vector concerned. We observe that the decaying of the amplitude of the concerned modes of  $\langle B_z \rangle_z$  and  $\langle \Phi \rangle_z$  is not perpetue, but until they reach a value that is naturally maintained by the turbulence (in our case it happens after about  $t = 6$ ).

The diffusion of  $B/\rho$  on large scales was also observed in Heitsch et al. (2004) for the two fluid simulations, but it was interpreted as arising from the difference between the velocity field of the ions and neutrals, at small scales. However, we also observe similar effect in our one-fluid simulations in the presence of the turbulent velocity field.

Figure 6 shows the distribution of  $\langle \rho \rangle_z$  versus  $\langle B_z \rangle_z$  and  $\langle \rho \rangle_z$  versus  $\langle \Phi \rangle_z$  for the model B2 ( $B_0 = 1.0$ ) at different time-steps ( $t = 0, 0.5$  and  $10$ ). We see in this projected view that the initial flux-mass relation is quickly spread and, in contrast with the  $\Phi - \rho$  distribution, we do not see any tendency for the magnetic field and density to become correlated.

To give a quantitative measure of the evolution of the flux-to-mass relation in the models, let us consider  $\langle \delta B, \delta \rho \rangle$ , the correlation between fluctuations of the magnetic field  $\delta B$  and density  $\delta \rho$ , defined by:

$$\langle \delta B, \delta \rho \rangle = \frac{\int (B - \bar{B})(\rho - \bar{\rho}) d^3x}{\sqrt{\int (B - \bar{B})^2 d^3x} \sqrt{\int (\rho - \bar{\rho})^2 d^3x}} \quad (15)$$

Figure 7 shows the evolution of  $\langle \delta B, \delta \rho \rangle$  (left) and  $\langle \delta \Phi, \delta \rho \rangle$  (right), which is similarly defined. Differently from the passive scalar field that quickly becomes correlated to the density field, the magnetic field seems to keep an anti-correlation with it.

A more careful analysis of our results indicates that there may be some weak correlations between magnetic field intensity and density. For example, when we calculate the correlation  $\langle \delta B, \delta \rho \rangle$  using the turbulent models of Table 1 studied in section §4, we find weak positive correlations for the supersonic models and negative cor-

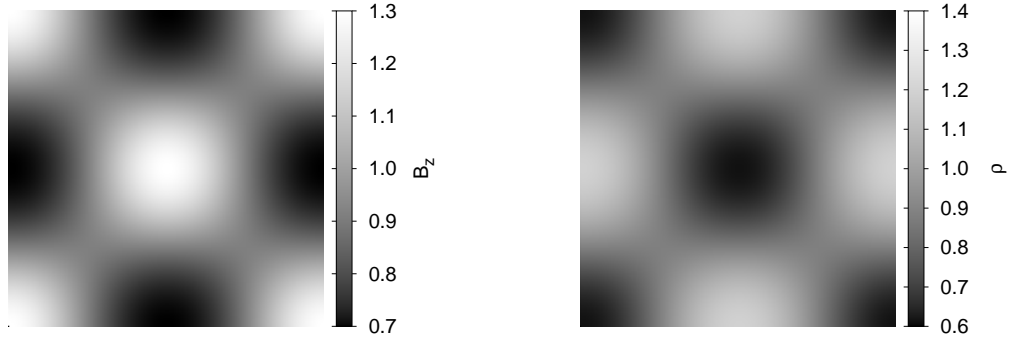


FIG. 3.—  $(x, y)$ -plane showing the initial configuration of the  $z$  component of the magnetic field  $B_z$  (left) and the density distribution (right) for the model B2 (see Table 2). The centers of the plots correspond to  $(x, y) = (0, 0)$ .

TABLE 2  
PARAMETERS OF THE SIMULATIONS IN THE STUDY OF TURBULENT DIFFUSION OF MAGNETIC FLUX WITHOUT GRAVITY.

Model	$B_0$	$l_{inj}$	$V_{rms}$	$t_{turb}$	$\eta_{turb} - B_z$	$\eta_{turb} - \Phi$	Resolution
B1	0.5	0.4	0.8	0.5	0.18(0.03)	0.19(0.02)	$256^3$
B2	1.0	0.4	0.8	0.5	0.09(0.02)	0.14(0.02)	$256^3$
B3	1.5	0.4	0.8	0.5	0.10(0.02)	0.08(0.02)	$256^3$
B4	2.0	0.4	0.8	0.5	0.13(0.02)	0.11(0.02)	$256^3$

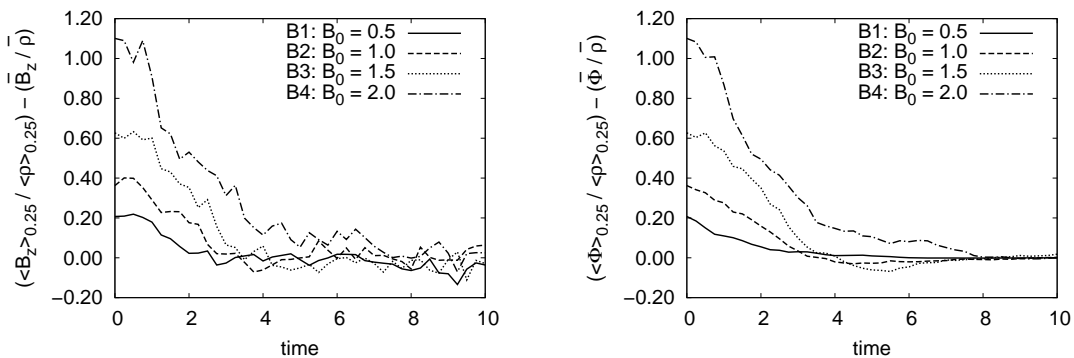


FIG. 4.— *Left*: Evolution of the ratio of the averaged magnetic field over the averaged density within a distance  $R = 0.25L$  from the central  $z$ -axis. *Right*: Evolution of the ratio of the averaged passive scalar over the averaged density. The values have been subtracted from their characteristic values  $\bar{B}/\bar{\rho}$  in the box.

relations for the subsonic ones. These correlations increase with  $M_A$ . Thus, the anti-correlation detected in Figure 7 can be due to the slightly subsonic regime of the turbulence. These correlations and anti-correlations at this level cannot be excluded by the observational data as discussed, e.g., in Troland & Heiles (1986). We shall address this issue in more detail elsewhere.

To summarize, the results of Figures 4 to 7 suggest that the turbulence can substantially change the flux-to-mass ratio  $B/\rho$  without any effect of ambipolar diffusion. The diffusion of the magnetic flux occurs in a rate similar to the rate of the turbulent diffusion of heat (passive scalar), even for sub-Alfvénic turbulence.

As remarked in section 2, we should emphasize that the efficient turbulent diffusion of magnetic field that we are observing in the simulations above are due to fast magnetic reconnection because otherwise, if the tangled magnetic lines by turbulence were not reconnecting, then they would be behaving like a jelly fluid and this would make the diffusive transport of magnetic flux very

inefficient (contrary to what is observed in the simulations). The issue of magnetic reconnection was avoided in Heitsch et al. (2004) due to the idealized settings. Magnetic reconnection, however, is an effect that any realistic 3D simulations of magnetized turbulent gas have to address.

## 6. TURBULENT DIFFUSION OF MAGNETIC FIELD IN THE PRESENCE OF GRAVITY

The turbulent diffusion of magnetic field in the absence of gravity can represent the magnetic field dynamics in diffuse interstellar gas where cloud self-gravity is not important. In molecular clouds, clumps and accretion disks, the diffusion of magnetic field should happen in the presence of gravity. We study this process below.

### 6.1. Numerical approach

In order to get an insight into the magnetic field diffusion in a turbulent fluid immersed in a gravitational potential, we have performed experiments in the presence



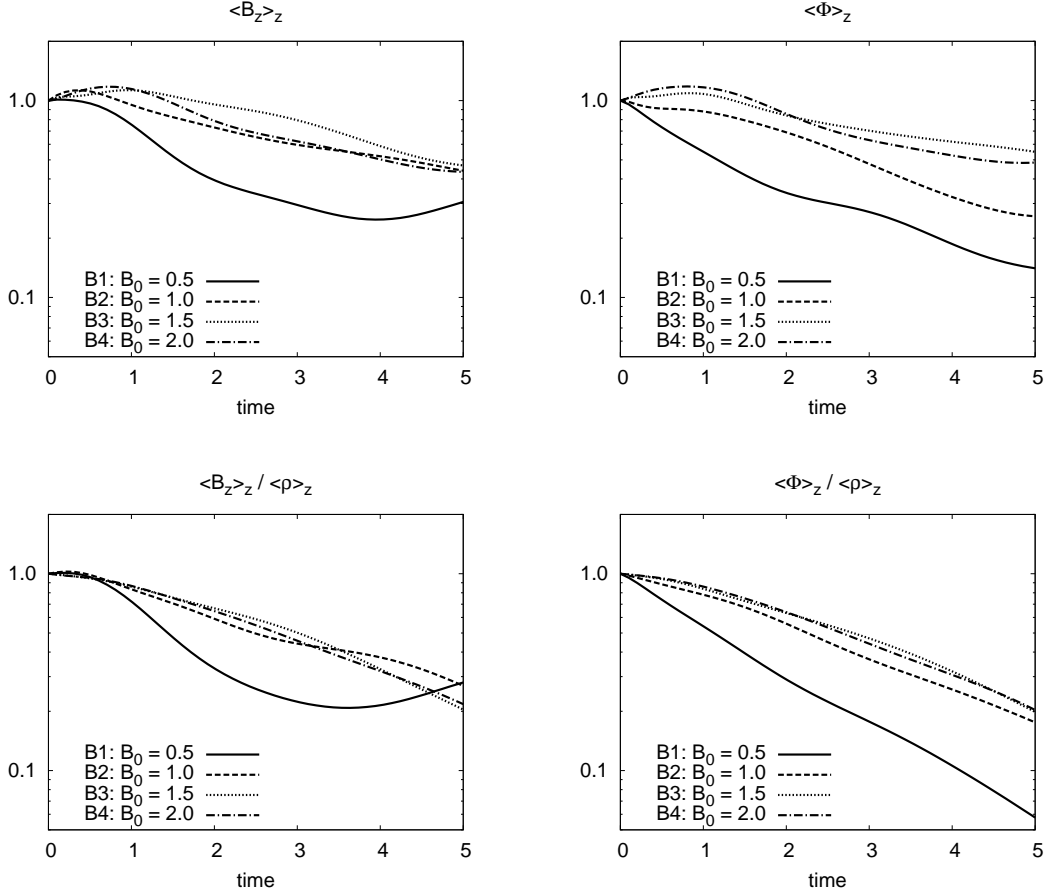


FIG. 5.— Evolution of the *rms* amplitude of the fourier modes  $(k_x, k_y) = (\pm 1, \pm 1)$  of  $\langle B_z \rangle_z$  (top left),  $\langle \Phi \rangle_z$  (top right),  $\langle B_z \rangle_z / \langle \rho \rangle_z$  (bottom left) and  $\langle \Phi \rangle_z / \langle \rho \rangle_z$  (bottom right). All the curves were smoothed to make the visualization clearer.

of a gravitational potential with cylindric symmetry  $\Psi$ , given in cylindrical coordinates  $(R, \phi, z)$  by:

$$\Psi(R \leq R_{max}) = -\frac{A}{R + R_*} \quad (16)$$

$$\Psi(R > R_{max}) = -\frac{A}{R_{max} + R_*} \quad (17)$$

where  $R = 0$  is the center of the  $(x, y)$ -plane, and we fixed  $R_* = 0.1L/2$  and  $R_{max} = 0.45L/2$  ( $L = 1$  is the size of the computational box, as remarked in §3). We assume a relatively high value of  $R_*$  in order to limit the values of the gravitational force and prevent the system to be initially Parker-Rayleigh-Taylor unstable. We assume an outer cut-off  $R_{max}$  on the gravitational force to keep the cylindrical symmetry while using periodic boundary conditions.

In one class of experiments, we start the simulation with a magneto-hydrostatic equilibrium with  $\beta = \frac{P_{gas}}{P_{mag}} = \frac{c_s^2 \rho}{B^2 / 8\pi}$  constant. The initial density and magnetic fields are, respectively:

$$\rho(R) = \rho_0 \exp \left\{ (\Psi(R_{max}) - \Psi(R)) / c_s^2 (1 + \beta^{-1}) \right\} \quad (18)$$

$$B_z(R) = c_s \sqrt{2\beta^{-1} \rho(R)} \quad (19)$$

Figure 8 illustrates this initial configuration for one of the studied models (model C2, see Table 3).

We restricted our experiments to the trans-sonic case  $c_s = 1$  (in most of the experiments, we keep  $V_{rms} \approx 0.8$ , see Table 3). We also fixed  $\rho_0 = 1$ . The turbulence is injected and we follow the evolution of  $\langle B_z \rangle_R$  and  $\langle \rho \rangle_R$  for 8 time-steps. Table 3 lists the parameters used for these experiments. The parameter  $A$  for the strength of the gravity is given in units of  $c_s^2 L$ .  $\bar{\rho}$  and  $\bar{B}_z$  represent the average of the density and magnetic field over the entire box.  $V_{A,i}$  refers to the initial Alfvén speed of the system. The *rms* velocity of the system  $V_{rms}$  is measured after the turbulence is well-developed.

We have also performed experiments starting out of equilibrium, with homogeneous fields: the system starts in free fall. We left the system to evolve for 8 time steps applying turbulence since the beginning. For a comparison, we have also performed these experiments without turbulence. The initial uniform magnetic field is parallel to the  $z$  direction for these models. Table 4 lists the parameters for these runs. The listed values of  $\beta$  refer to the initial conditions.

Concerning the diffusion of the magnetic field, in order to provide a quantitative comparison between the models, we have also performed simulations with similar initial conditions to the models presented in Table 3, but without turbulence and with the explicit presence of Ohmic diffusivity  $\eta_{Ohm}$  in the induction equation. As these models have perfect symmetry in the  $z$ -direction,

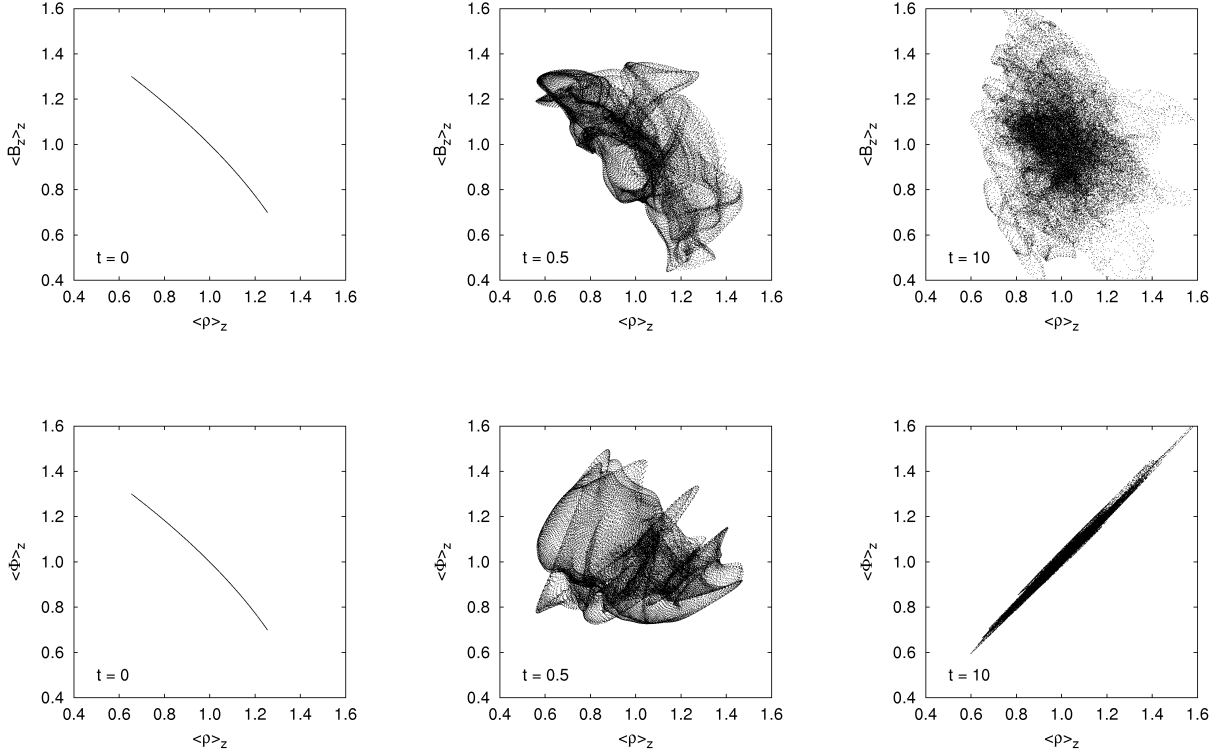


FIG. 6.— Distribution of  $\langle \rho \rangle_z$  versus  $\langle B_z \rangle_z$  (top row) and  $\langle \rho \rangle_z$  versus  $\langle \Phi \rangle_z$  (bottom row) for model B2 (see Table 2), at  $t = 0$  (left),  $t = 0.5$  (middle) and  $t = 10$  (right).

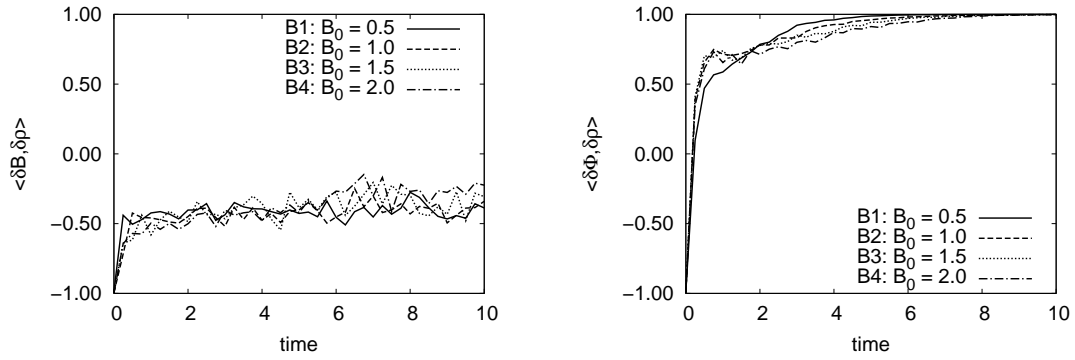


FIG. 7.— *Left*: Correlation between fluctuations of the strength of the magnetic field ( $\delta B$ ) and density ( $\delta \rho$ ). *Right*: Correlation between fluctuations of the passive scalar field ( $\delta \Phi$ ) and density ( $\delta \rho$ ).

we simulated only a plane cutting the  $z$ -axis, that is, they are 2.5D simulations. We use a resolution comparable to the turbulent 3D models. Table 5 lists the parameters for these runs. We simulated a three-dimensional model equivalent to the model E7r1, and we found exact agreement in the time evolution of the magnetic flux distribution (not showed). Therefore we can believe that these 2.5D simulations give results which are equivalent to 3D simulations.

## 6.2. Results

### 6.2.1. Evolution of the equilibrium distribution

Top row of Figure 9 shows the evolution of  $\langle B_z \rangle_{0.25}$  (left),  $\langle \rho \rangle_{0.25}$  (middle) and  $\langle B_z \rangle_{0.25} / \langle \rho \rangle_{0.25}$  (right), normalized by the respective characteristic values inside the

box ( $\bar{B}_z$ ,  $\bar{\rho}$  and  $\bar{B}_z / \bar{\rho}$ ), for the models C1, C2, and C3 ( $\beta = 1$ ). We compare the evolution of these quantities for different strengths of gravity  $A$ , maintaining the other parameters identical. The central magnetic flux reduces faster the higher the value of  $A$ . The flux-to-mass ratio has similar behavior. The other rows of Figure 9 show the profile of the quantities  $\langle B_z \rangle_z$  (left),  $\langle \rho \rangle_z$  (middle), and  $\langle B_z \rangle_z / \langle \rho \rangle_z$  (right) along the radius  $R$ , each row corresponding to a different value of  $A$  both for  $t = 0$  (in magneto-hydrostatic equilibrium and constant  $\beta$ ) and for  $t = 8$ . We see a deeper decaying of the magnetic flux toward the central region for the highest values of  $A$  at  $t = 8$ .

In Figure 10, we compare the behavior of the diffusion when we change the turbulent velocity and maintain the

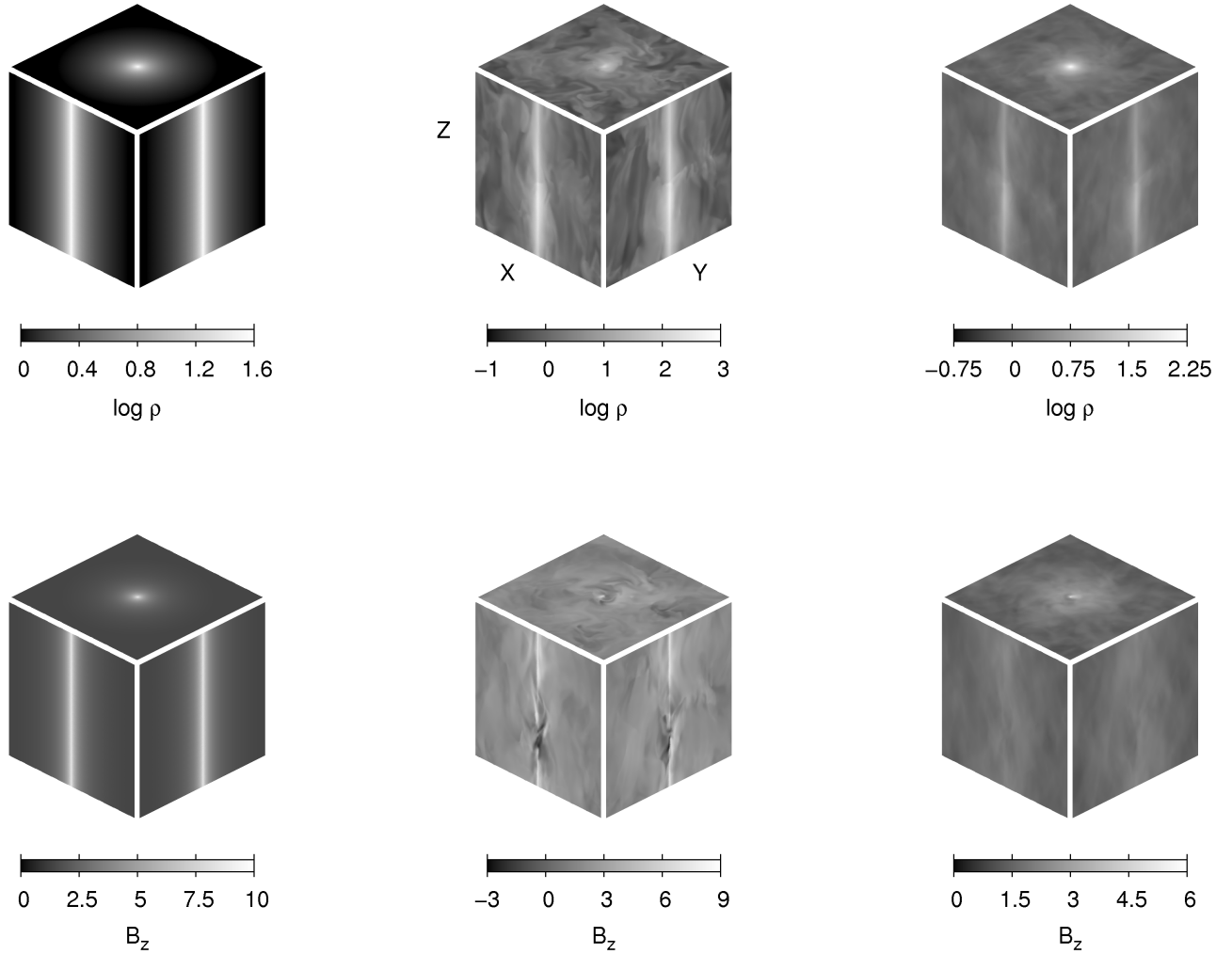


FIG. 8.— Model C2 (see Table 3). *Top row*: logarithm of the density field; *Bottom row*:  $B_z$  component of the magnetic field. *Left column*: central  $xy$ ,  $xz$ , and  $yz$  slices of the system projected on the respective walls of the cubic computational domain, in  $t = 0$ ; *middle column*: the same for  $t = 3$ ; *right column*: the  $xy$  wall shows the averaged quantity integrated over the  $z$ -direction; the  $yz$  wall: the averaged quantities integrated over the  $x$ -direction, and the  $xz$  wall shows the averaged quantities integrated over the  $y$ -direction, in  $t = 3$ .

TABLE 3  
PARAMETERS FOR THE MODELS STARTING AT MAGNETO-HYDROSTATIC EQUILIBRIUM WITH INITIAL CONSTANT  $\beta$ .

Model	$\beta^1$	$V_{A,i}$	$A^2$	$\bar{\rho}$	$B_z$	$V_{rms}$	$t_{turb}$	$\eta_{turb}$	$\eta_{turb}/V_{rms}l_{inj}$	Resolution
C1	1.0	1.4	0.6	1.26	1.59	0.8	0.5	$\lesssim 0.005$	$\lesssim 0.015$	$256^3$
C2	1.0	1.4	0.9	1.52	1.74	0.8	0.5	$\approx 0.01$	$\approx 0.03$	$256^3$
C3	1.0	1.4	1.2	1.95	1.98	0.8	0.5	$\approx 0.03$	$\approx 0.09$	$256^3$
C4	1.0	1.4	0.9	1.52	1.74	1.4	0.3	$\approx 0.10 - 0.20$	$\approx 0.18 - 0.36$	$256^3$
C5	1.0	1.4	0.9	1.52	1.74	2.0	0.2	$\gtrsim 0.30$	$\gtrsim 0.37$	$256^3$
C6	3.3	0.8	0.9	2.40	1.20	0.8	0.5	$\approx 0.02$	$\approx 0.06$	$256^3$
C7	0.3	2.4	0.9	1.18	2.66	0.8	0.5	$\approx 0.01$	$\approx 0.03$	$256^3$

<sup>a</sup>Initial  $\beta$  parameter for the plasma:  $\beta = \frac{P_{gas}}{P_{mag}} = \frac{c_s^2 \bar{\rho}}{B^2/8\pi}$

<sup>b</sup>The parameter  $A$  for the strength of gravity (see Equations 16 and 17) is given in units of  $c_s^2 L$ .

other parameters identical as in models C2, C4 and C5. An inspection of the left panel shows that the central magnetic flux  $\langle B_z \rangle_{0,25}$  decays faster (and almost equally)

for the two highest turbulent velocities. Fluctuations are higher in the cases with highest velocity. The central density however, is smaller with the increase of the tur-

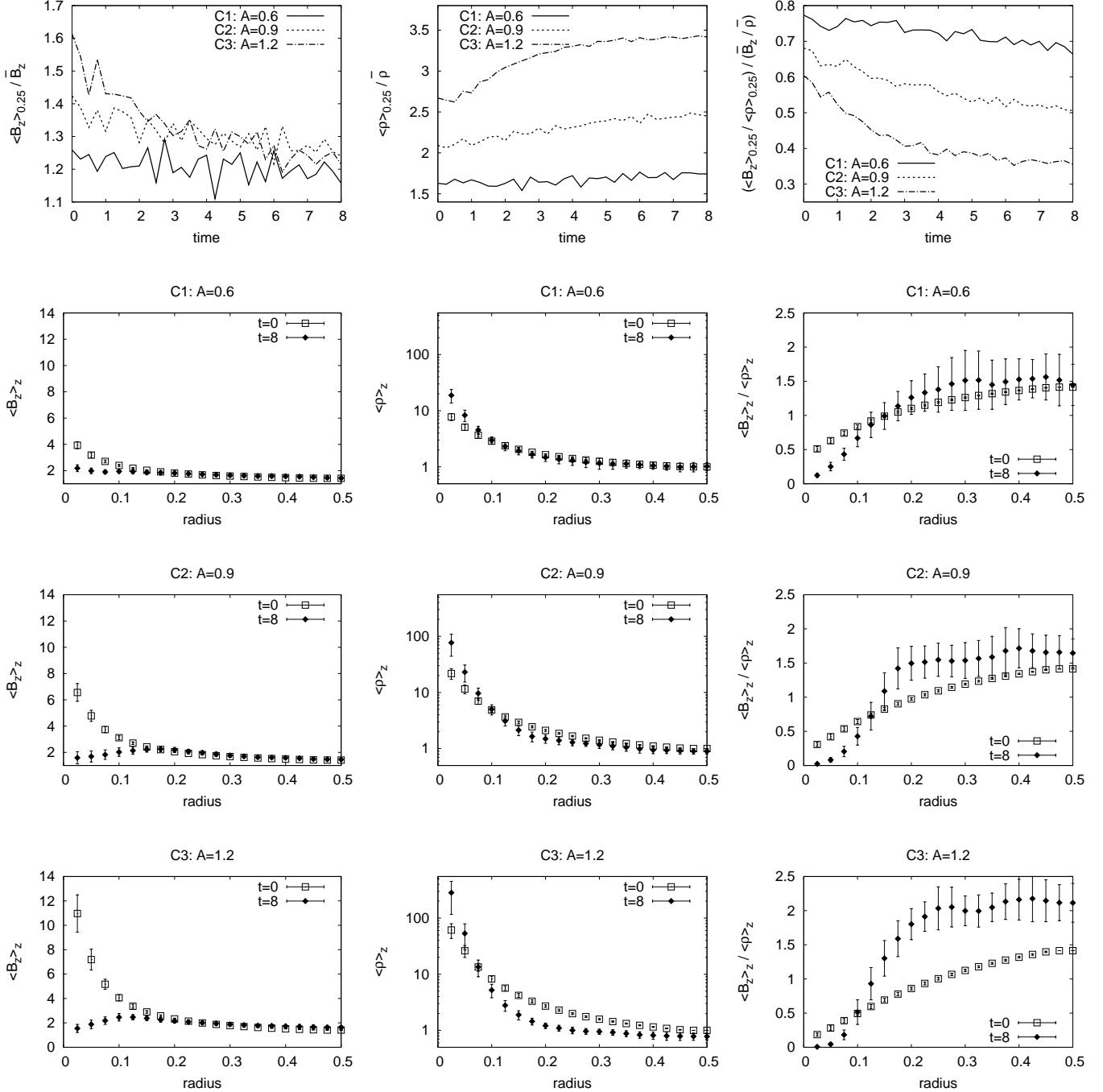


FIG. 9.— The top row shows the time evolution of  $\langle B_z \rangle_{0.25} / \bar{B}_z$  (left),  $\langle \rho \rangle_{0.25} / \bar{\rho}$  (middle), and  $(\langle B_z \rangle_{0.25} / \langle \rho \rangle_{0.25}) / (\bar{B}_z / \bar{\rho})$  (right). The other rows show the radial profile of  $\langle B_z \rangle_z$  (left),  $\langle \rho \rangle_z$  (middle), and  $\langle B_z \rangle_z / \langle \rho \rangle_z$  (right) for the different values of  $A$  in  $t = 0$  (magneto-hydrostatic solution with  $\beta$  constant, see Table 3) and  $t = 8$ . Error bars show the standard deviation. All models have initial  $\beta = 1.0$ .

bulent velocity. This is explained by the fact that the dynamic pressure is higher for the largest velocities. The central flux-to-mass ratio  $\langle B_z \rangle_{0.25} / \langle \rho \rangle_{0.25}$  decays for the two smallest velocities. However, for the largest velocity, it is not clear if this ratio decays or not. Looking at the middle graph of Figure 10 (*bottom row*), we see that the central density decreases for the highest forcing. This is indicative that the turbulence driving overcomes the gravitational potential making the system less bound. In

this situation we do expect the magnetic field and density to lose their correlation, as we have seen in §5.

Top row of Figure 11 compares the evolution of  $\langle B_z \rangle_{0.25}$  (left),  $\langle \rho \rangle_{0.25}$  (middle) and  $\langle B_z \rangle_{0.25} / \langle \rho \rangle_{0.25}$  (right), normalized by the respective characteristic average values inside the box ( $\bar{B}_z$ ,  $\bar{\rho}$  and  $\bar{B}_z / \bar{\rho}$ ), for models C2, C6, and C7 with different  $\beta$ . Both the central magnetic flux and the flux-to-mass ratio decay faster for the less magnetized model ( $\beta = 3.3$ ). The other rows

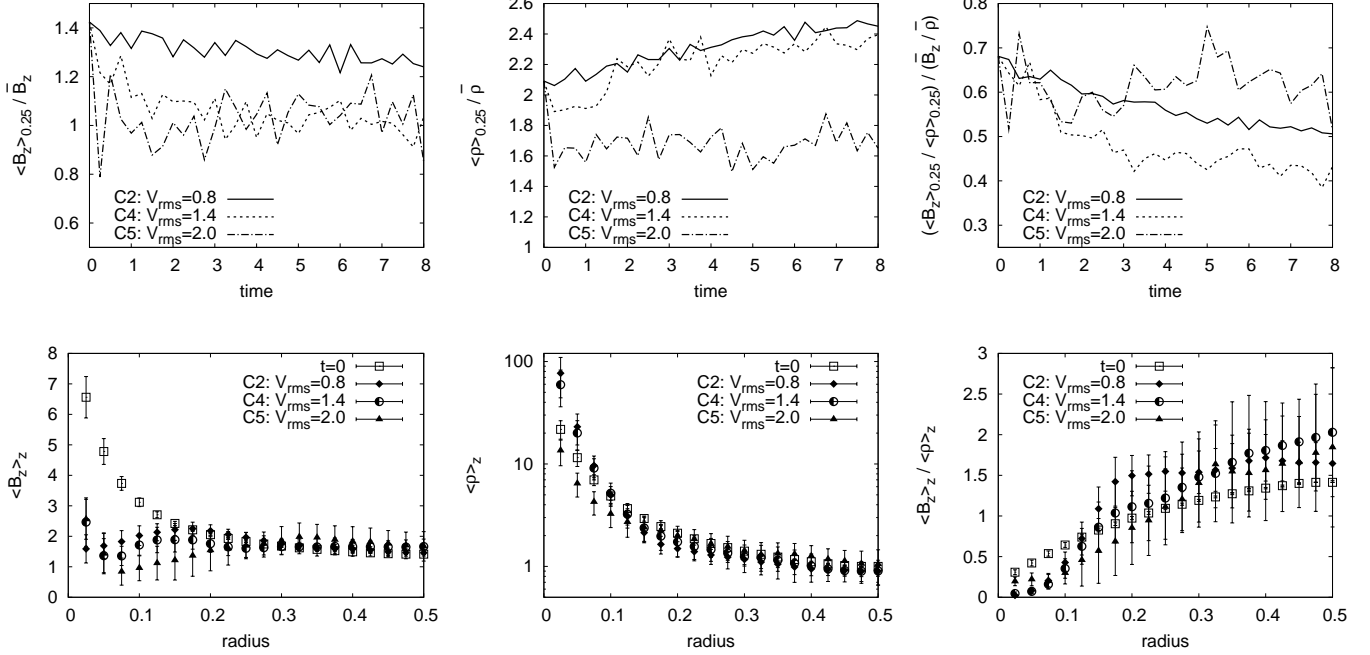


FIG. 10.— The top row shows the time evolution of  $\langle B_z \rangle_{0.25} / \bar{B}_z$  (left),  $\langle \rho \rangle_{0.25} / \bar{\rho}$  (middle), and  $(\langle B_z \rangle_{0.25} / \langle \rho \rangle_{0.25}) / (\bar{\rho} / \bar{B}_z)$  (right). The bottom row shows the radial profile of  $\langle B_z \rangle_z$  (left),  $\langle \rho \rangle_z$  (middle), and  $\langle B_z \rangle_z / \langle \rho \rangle_z$  (right) for each value of the turbulent velocity  $V_{rms}$ , in  $t = 0$  (magneto-hydrostatic solution with  $\beta$  constant) and  $t = 8$ . Error bars show the standard deviation. All models have initial  $\beta = 1.0$ . See Table 3.

TABLE 4  
PARAMETERS FOR THE EXPERIMENTS STARTING  
OUT-OF-EQUILIBRIUM, WITH INITIALLY HOMOGENEOUS FIELDS.

Model	$\beta$	$V_{A,i}$	A	$\bar{\rho}$	$\bar{B}_z$	$V_{turb}$	Resolution
D1	1.0	1.4	0.9	1.0	1.41	0.8	$256^3$
D1a	1.0	1.4	0.9	1.0	1.41	0.0	$256^3$
D2	3.3	0.8	0.9	1.0	0.77	0.8	$256^3$
D2a	3.3	0.8	0.9	1.0	0.77	0.0	$256^3$
D3	0.3	2.4	0.9	1.0	2.45	0.8	$256^3$
D3a	0.3	2.4	0.9	1.0	2.45	0.0	$256^3$

TABLE 5  
PARAMETERS FOR THE 2.5D RESISTIVE MODELS STARTING WITH  
MAGNETO-HYDROSTATIC EQUILIBRIUM AND CONSTANT  $\beta$ .

Model	$\beta$	A	$\eta_{Ohm}$	Resolution
E1r0	1.0	0.6	0.005	$256^2$
E1r1	1.0	0.6	0.01	$256^2$
E2r1	1.0	0.9	0.01	$256^2$
E2r2	1.0	0.9	0.02	$256^2$
E2r3	1.0	0.9	0.03	$256^2$
E2r4	1.0	0.9	0.05	$256^2$
E3r1	1.0	1.2	0.01	$256^2$
E3r2	1.0	1.2	0.02	$256^2$
E3r3	1.0	1.2	0.03	$256^2$
E4r2	1.0	0.9	0.10	$256^2$
E4r3	1.0	0.9	0.20	$256^2$
E5r3	1.0	0.9	0.30	$256^2$
E6r1	3.3	0.9	0.01	$256^2$
E6r2	3.3	0.9	0.02	$256^2$
E6r3	3.3	0.9	0.03	$256^2$
E7r1	0.3	0.9	0.01	$256^2$

of Figure 11 show the radial profile of the quantities  $\langle B_z \rangle_z$  (left),  $\langle \rho \rangle_z$  (middle) and  $\langle B_z \rangle_z / \langle \rho \rangle_z$  (right) for

each model. We can again observe a lower value of the flux in the central region (relative to the external regions) for the highest values of  $\beta$  at the time step  $t = 8$ . The contrast between the central and the more external values for the flux-to-mass ratio is quite different for the three models, being higher for the more magnetized models. This is expected, as turbulence brings the system in the state of minimal energy. The effect of varying magnetization in some sense is analogous to the effect of varying gravity. The equilibrium contrast of flux-to-mass ratio is larger in both the case of higher gravity and higher magnetization. The physics is simple, the lighter fluid (magnetic field) gets segregated from the heavier fluid (gas).

All in all, we clearly see that turbulence substantially influences the quasi-static evolution of magnetized gas in the gravitational potential. The system in the presence of turbulence relaxes fast to its minimum potential energy state. This explains the change of the flux-to-mass ratio, which for years was a problem to deal with invoking ambipolar diffusion.

We should note that in order to test resolution effects, we have also performed simulations of model C2 using both higher ( $512^3$ ) and smaller ( $128^3$ ) resolutions than  $256^3$  and obtained essentially the same results as those presented.

### 6.2.2. Equilibrium distribution: Comparison of magnetic diffusivity and resistivity effects

In terms of the removal of the magnetic field from quasi-static clouds, is the effect of turbulent magnetic diffusion similar to the effect of diffusion of magnetic field due to Ohmic effects? To address this question, we have performed a series of simulations with enhanced Ohmic resistivity (see models of Table 5).

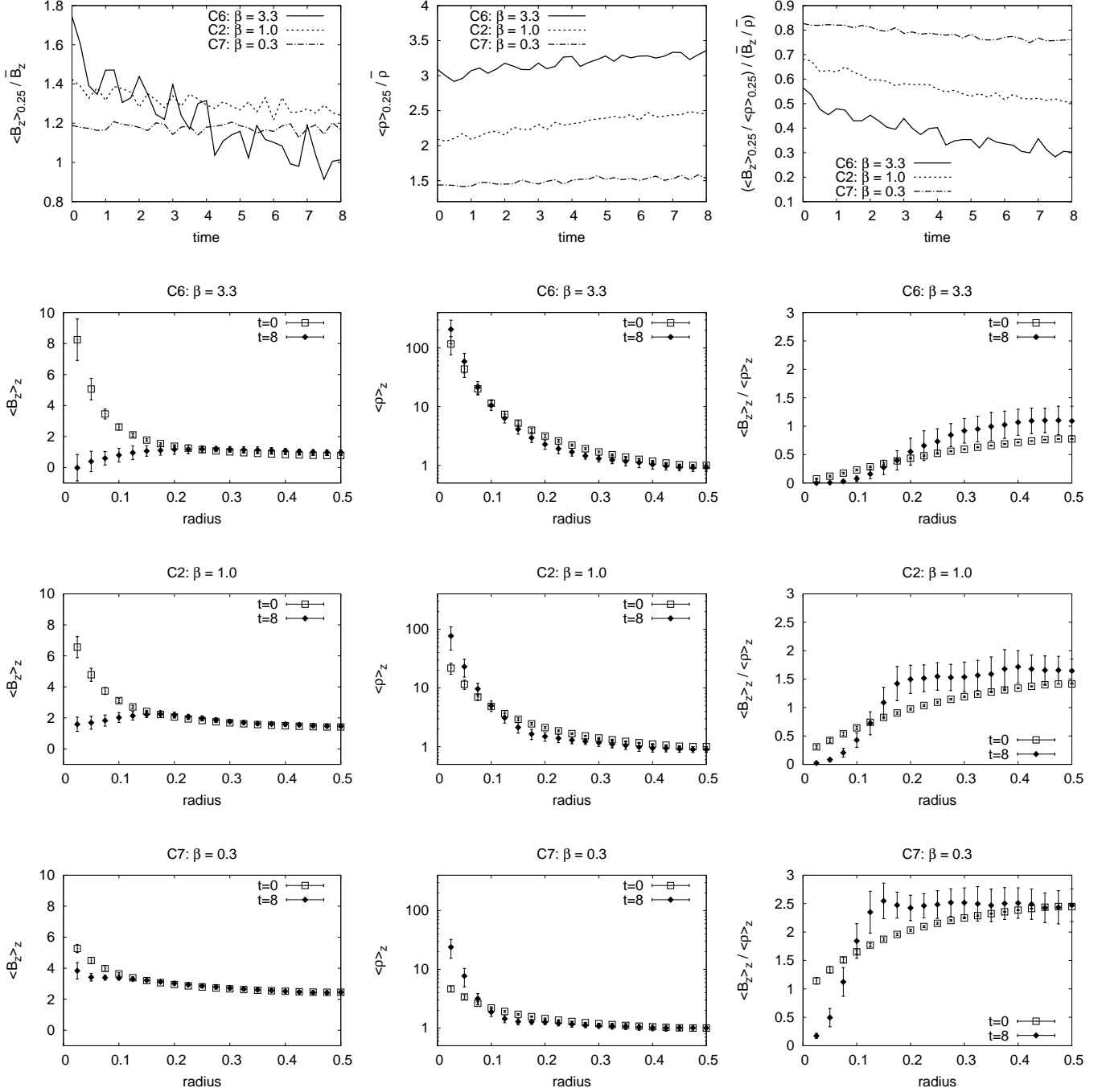


FIG. 11.— The top row shows the time evolution of  $\langle B_z \rangle_{0.25} / \bar{B}_z$  (left),  $\langle \rho \rangle_{0.25} / \bar{\rho}$  (middle), and  $(\langle B_z \rangle_{0.25} / \langle \rho \rangle_{0.25}) / (\bar{B}_z / \bar{\rho})$  (right). The other rows show the radial profile of  $\langle B_z \rangle_z$  (left),  $\langle \rho \rangle_z$  (middle), and  $\langle B_z \rangle_z / \langle \rho \rangle_z$  (right) for each value of  $\beta$ , in  $t = 0$  (magneto-hydrostatic solution with  $\beta$  constant) and  $t = 8$ . Error bars show the standard deviation of the data. See Table 3.

In Figure 12 we compare the evolution of  $\langle B_z \rangle_R$  (at different radius) for model C2 of Table 3 with similar resistive models without turbulence of Table 5, with different values of Ohmic diffusivity  $\eta_{Ohm}$ . The decaying seems initially faster and comparable with the highest value of  $\eta_{Ohm}$  ( $\eta_{Ohm} = 0.05$ ). But after this initial phase, the turbulent model (C2) seems to have a behaviour similar to the resistive models with  $\eta_{Ohm} 0.01 - 0.02$ .

Figure 13 compares the turbulent models C1 (*top row*) and C3 (*bottom row*) of Table 3 with similar resistive

models of Table 5. After roughly one time step, the model C1 (weaker gravitational field) seems to be consistent with a value of  $\eta_{Ohm}$  between 0.005 or lesser, while the model C3 (stronger gravitational field) seems to be consistent with  $\eta_{Ohm} \approx 0.03$ . These results show that the effective turbulent magnetic diffusivity is sensitive to the strength of the gravitational field.

Figure 14 shows similar comparisons as in Figure 13 for the turbulent models C4 (*top row*) and C5 (*bottom row*) (see Table 3) with resistive models without turbulence

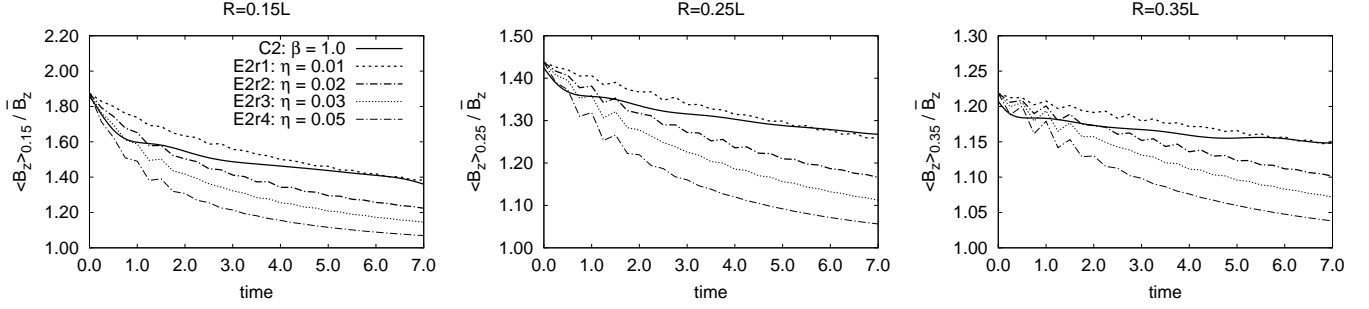


FIG. 12.— Comparison between the model C2 (turbulent diffusivity) and resistive models without turbulence (see Table 5). All the cases have analogous parameters. The curve for the model C2 was smoothed here for the sake of clarity.

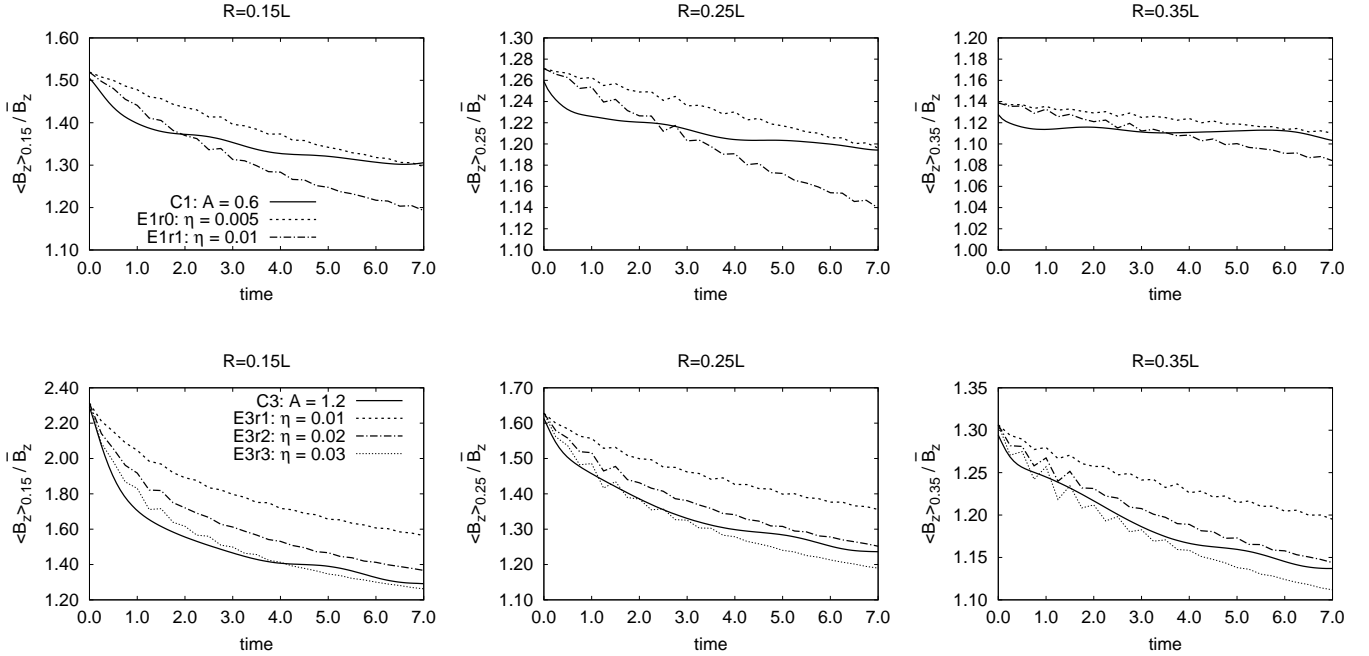


FIG. 13.— Comparison of the models C1 (*top row*) and C3 (*bottom row*) (see Table 3) with resistive models without turbulence (see Table 5). The curves for the models C1 and C3 were smoothed here for better clarity.

of Table 5. The most comparable resistive simulations have increasing  $\eta_{Ohm}$  values with increasing turbulent velocity. The model C4 (with smaller turbulent velocity) seems to be consistent with the resistive model with  $\eta_{Ohm} = 0.10$ . For the model C5 (with larger turbulent velocity), the curve with  $\eta_{Ohm} \sim 0.30$  (or higher) is more comparable; however, in this case we can not have a representative value of  $\eta_{Ohm}$  due to the very quick diffusion which occurs even before  $t = 1$ , when the turbulence becomes well developed.

Figure 15 compares the evolution of turbulent models with different magnetizations, models C6 and C7 (see Table 3), with resistive models of Table 5. The turbulent curve for the less magnetized model (C6) seems to follow the resistive curve with  $\eta_{Ohm} = 0.02$ , while the more magnetized model (C7) is comparable to the resistive model with  $\eta_{Ohm} \approx 0.01$ . This result indicates that the effective turbulent diffusivity is also sensitive to the strength of the magnetic field.

In summary, the results above indicate a correspon-

dence between the two different effects. In other words, the turbulent magnetic diffusion may mimic the effects of Ohmic decay of magnetic fields in gravitating clouds. However, we should keep in mind that the physics of turbulent diffusion and Ohmic resistivity is different. Thus this analogy should not be overstated.

### 6.2.3. Evolution of non-equilibrium models

Figure 16 shows the same set of comparisons as in Figure 11 for the models D1, D2, and D3 of Table 4 — these models have started out of the equilibrium with homogeneous density and magnetic fields in a free fall system. Besides the runs with turbulence, we also present, for comparison, the evolution for the systems without turbulence (models D1a, D2a, and D3a). The strong oscillations seen in the evolution of the central magnetic flux and density for these models (which are more pronounced in the models without turbulence) are acoustic oscillations, since the time for the virialization of these systems is larger than the simulated period. We note that the initial flux-to-mass ratio does not change in the

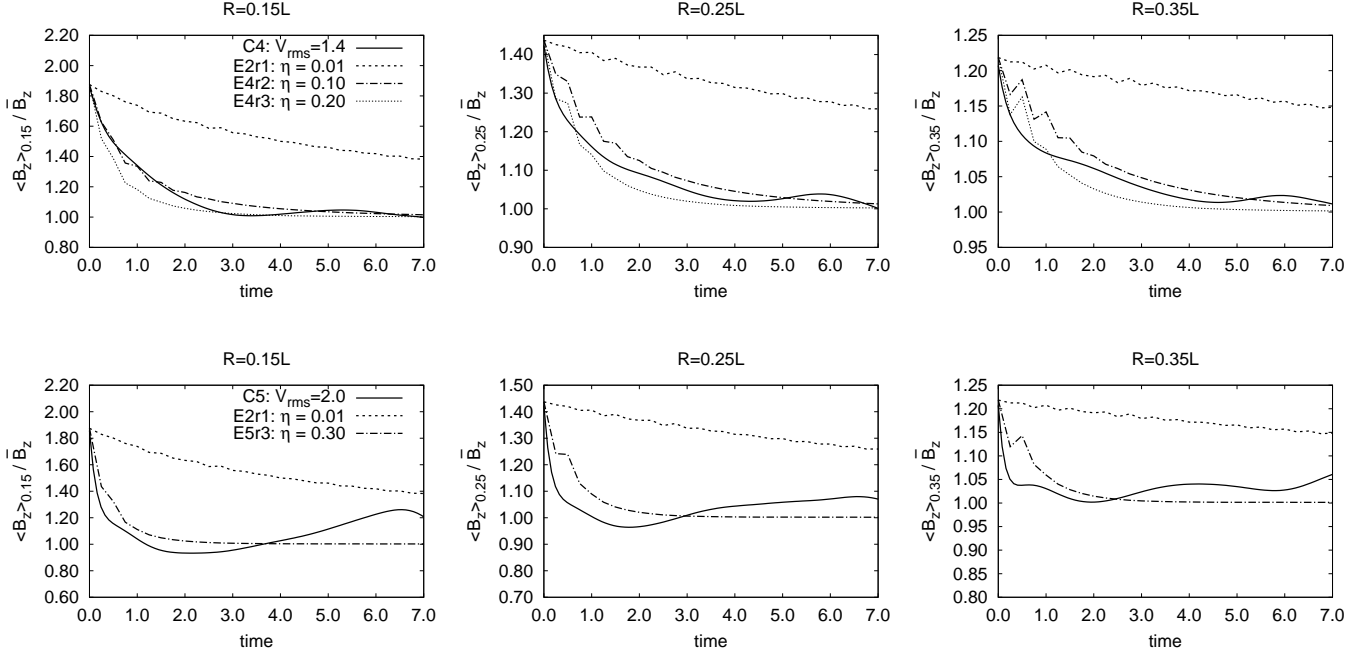


FIG. 14.— Comparison of the models C4 (*top row*) and C5 (*bottom row*) (see Table 3) with resistive models without turbulence (see Table 5). The curves for the models C4 and C5 were also smoothed here.

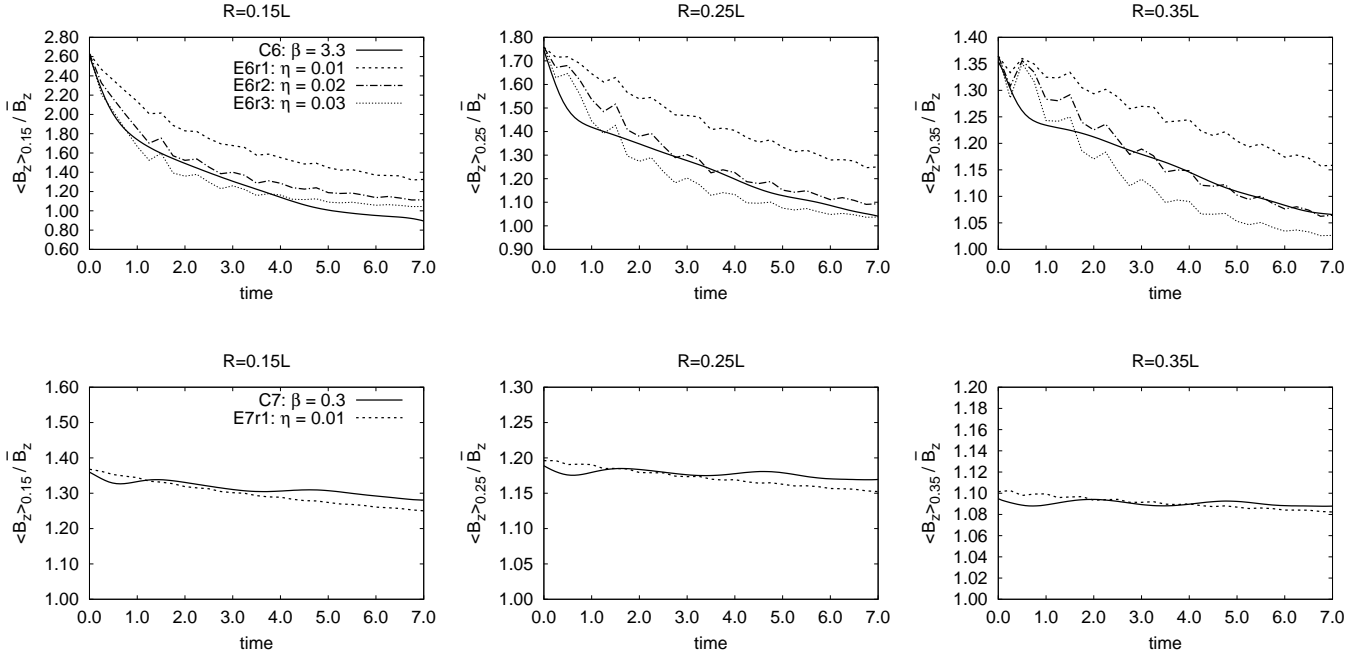


FIG. 15.— Comparison between the models C6 (*top row*) and C7 (*bottom row*) (see Table 3) with resistive models without turbulence (see Table 5). The curves for the models C6 and C7 were smoothed here.

cases without turbulence. We also observe similar trends as in Figure 11: the higher the value of  $\beta$ , the faster the decay of the central magnetic flux relative the mean flux into the box. We also note that the radial profile of the flux-to-mass ratio for the turbulent models crosses the mean value for the models without turbulence at nearly the same radius. This is due to the fact that the effective gravity potential in all these simulations acts up to this

radius approximately.

This set of simulations shows that the change of mass-to-flux ratio can happen at the time scale of the gravitational collapse of the system and therefore, turbulent diffusion of magnetic field is applicable to dynamic situations, e.g. to the formation of supercritical cores.

### 6.3. Magnetic field expulsion revealed



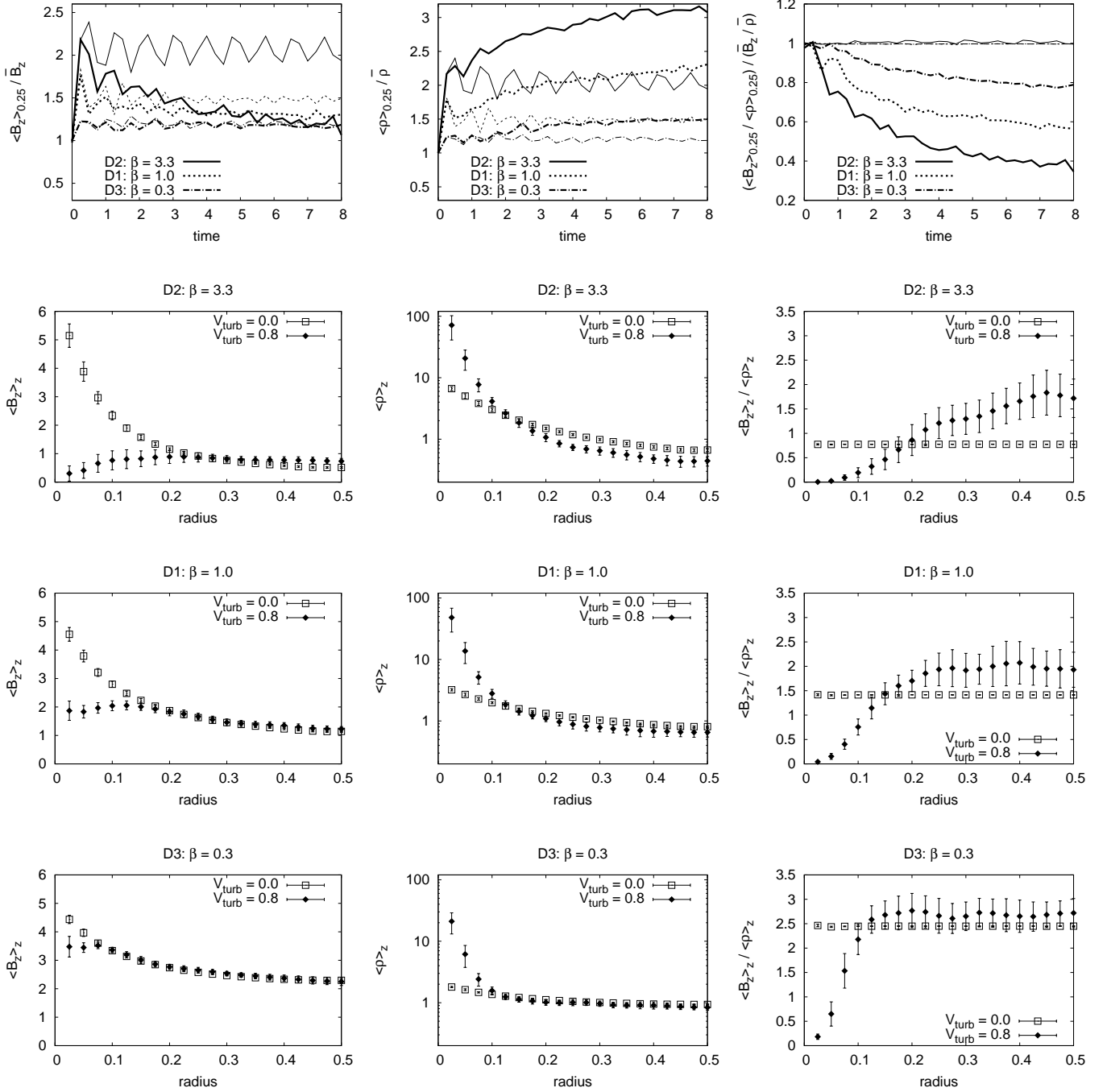


FIG. 16.— The top row shows the time evolution of  $\langle B_z \rangle_{0.25} / \bar{B}_z$  (left),  $\langle \rho \rangle_{0.25} / \bar{\rho}$  (middle), and  $(\langle B_z \rangle_{0.25} / \langle \rho \rangle_{0.25}) / (\bar{B}_z / \bar{\rho})$  (right), for runs with (thick lines) and without (thin lines) injection of turbulence. The other rows show the radial profile of  $\langle B_z \rangle_z$  (left),  $\langle \rho \rangle_z$  (middle) and  $\langle B_z \rangle_z / \langle \rho \rangle_z$  (right) for different values of  $\beta$ , in  $t = 8$ , for runs with and without turbulence. Error bars show the standard deviation. See Table 4.

Both in the case of equilibrium and non-equilibrium we observe a substantial change of the mass-to-flux ratio. Even our experiments with no turbulence injection confirm that this process arises from the action of turbulence. As a result, in all the cases with gravity involved the turbulence allows magnetic field to escape from the dense core which is being formed in the center of the gravitational potential.

## 7. DISCUSSION OF THE RESULTS: RELATIONS TO EARLIER STUDIES

Through this work we have performed the comparison of our results with the studies by Cho et al. (2003) and Heitsch et al. (2004). Below, we provide yet another outlook of the connection of these studies with the present paper. We also discuss the work by Shu et al. (2006), which was the initial motivation of our study of the diffusion of magnetic field in the presence of gravity.

### 7.1. Comparison with Cho et al. (2003)

In order to compare directly the present results with those in the previous work by Cho et al. (2003), we should remark a different detail in the setup used in that work: the size of the computational box  $L$  used there is  $2\pi$ , the injection scale  $l_{inj} \sim L/2.5$  and the turbulent velocity  $v_{turb} \sim 1$ , giving the characteristic turbulent time (the circulation time for the largest eddies)  $t_{turb} \sim l_{inj}/v_{turb} \approx 2.5$  time steps in code units. In the present experiments, the turbulent time is  $t_{turb} \sim 0.4$  time steps in code units.

Keeping this difference in mind, our results, which are of compressible MHD and were performed with higher resolution are roughly consistent with the findings in Cho et al. (2003). Our results show that the turbulent diffusivity of passive scalar fields  $\eta_{turb}$  is well described by  $\eta_{turb} = C_* v_{turb} l_{inj}$ , similar to the hydrodynamic case, and that the coefficient  $C_*$  is not very sensitive to the strength of the magnetic field. Therefore, the magnetic field does not impose a strong suppression of the turbulent diffusion perpendicular to it as far as heat transfer is concerned.

As already pointed in Cho et al. (2003) (see also Lazarian 2006), the effectiveness of the turbulent diffusion has important consequences on the thermal diffusion in the ISM and ICM. The nearly isotropic turbulent diffusivity can be one order of magnitude higher in the gas of central regions of galaxy clusters, like the Hydra A cluster, compared to the Spitzer value, based on the kinetic theory. In the ISM, in mixing layers, where turbulence is very strong, the turbulent diffusivity can be two orders of magnitude higher than the laminar values (see Esquivel et al. 2006). Our results extend the range of the applicability of the turbulent heat advection model of Cho et al. (2003).

### 7.2. Comparison with Heitsch et al. (2004): ambipolar diffusion versus turbulence and 2.5D versus 3D

As we discussed earlier, Heitsch et al. (2004) studied the turbulent ambipolar diffusion of the magnetic field through neutral matter using 2.5D simulations with a prescribed chaotic velocity field (of single scale) for the neutral matter.

In view of astrophysical implications, the comparison between our results and those of Heitsch et al. (2004) calls for the discussion on how ambipolar diffusion and turbulence interact to affect the magnetic field diffusivity. One way is to view the two processes as synergetic, acting coherently to speed up magnetic field diffusion. Indeed, one can argue that turbulence mixes up magnetic fields and matter on large scale, while ambipolar diffusion enables fast magnetic field diffusion on the small scales. In this situation it is not just “ambipolar diffusion”, not just “turbulent diffusion”, but a new process “turbulent ambipolar diffusion” that acts to enable fast magnetic diffusivity. This is a possible interpretation of the results of Heitsch et al. (2004).

At the same time, our results do not seem to exhibit less magnetic diffusivity than those of Heitsch et al. (2004). How can this be understood? In the absence of ambipolar diffusion, the turbulence propagates to smaller scales, increasing the turbulent diffusivity. On the other hand, ambipolar diffusion affects the turbulence, increas-

ing the damping scale. As a result, the ambipolar diffusion acts in two ways, in one to increase the small-scale diffusivity of the magnetic field, in another to decrease the turbulent small-scale diffusivity and these effects essentially compensate each other.

In other words, if we approximate the turbulent diffusivity by  $(1/3)V_{inj}L_{inj}$ , where  $V_{inj}$  and  $L_{inj}$  are the turbulent injection velocity and the injection scale, respectively, the ambipolar diffusivity acting on small scales will not play any role and the diffusivity will be purely “turbulent”. If, however, the ambipolar diffusion coefficient is larger than  $V_{inj}L_{inj}$ , then the Reynolds number of the steered flow may become small for turbulence to exist and the diffusion is purely ambipolar in this case. We believe that this leaves little if any parameter space for the “turbulent ambipolar diffusion” when turbulence and ambipolar diffusion synergetically enhance diffusivity, acting in unison. This point may be tested by 3D two-fluid simulations exhibiting both ambipolar diffusion and turbulence.

In view of our findings one may ask whether it is surprising to observe the diffusivity of magnetic field being independent of ambipolar diffusion in the case when turbulence is present. We can appeal to the fact well known in hydrodynamics, namely, that in a turbulent fluid the diffusion of a passive contaminant does not depend on the microscopic diffusivity. In the case of high microscopic diffusivity, the turbulence provides mixing down to a scale  $l_1$  at which the microscopic diffusivity both, suppresses the cascade and ensures efficient diffusivity of the contaminant. In the case of low microscopic diffusivity, turbulent mixing happens down to a scale  $l_2 \ll l_1$ , which ensures that even low microscopic diffusivity is sufficient to provide efficient diffusion. In both cases the total effective diffusivity of the contaminant is turbulent, i.e. is given by the product of the turbulent injection scale and the turbulent velocity. This analogy is not directly applicable to ambipolar diffusion, as this is a special type of diffusion and magnetic fields are different from passive contaminants (see §5). However, our results are indicative that to some extent the concepts of turbulent diffusion developed in hydrodynamics carries over to magnetized fluid.

### 7.3. Relation to Shu et al. (2006): fast removal of magnetic flux during star formation

As discussed in Shu et al. (2006), there is controversy about the ambipolar diffusion efficiency in accreting proto-stars. They have found that the dissipation should be about four orders of magnitude larger than the Ohmic dissipation in order to solve the magnetic flux problem in these systems. They then appealed to a hyper-resistivity concept in order to explain the higher dissipation of magnetic field in a turbulent environment.

We feel, however, that the hyper-resistivity idea is poorly justified (see criticism of it in Lazarian et al. 2004 and Kowal et al. 2009). At the same time, fast 3D reconnection can provide the magnetic diffusivity that is required for removal of the magnetic flux. This is what, in fact, was demonstrated in the present set of numerical simulations.

It is worth mentioning that, unlike the actual Ohmic diffusivity, magnetic diffusivity mediated by fast reconnection does not transfer the magnetic energy directly

into heat. The lion share of the energy is being released in the form of kinetic energy, driving turbulence. If the system is initially laminar, this potentially can result in flares of reconnection and the corresponding diffusivity. This is in agreement with LV99 scheme where a more intensive turbulence should induce more intensive turbulent energy injection and lead to the unstable feeding of the energy of the deformed magnetic field. However, the discussion of this effect is beyond the scope of the present paper.

Similar to Shu et al. (2006), we expect to observe the heating of the media. Indeed, although we do not expect to have Ohmic heating, the kinetic energy released due to magnetic reconnection is dissipated locally and therefore we expect to observe heating in the medium.

Our setup for gravity can be seen as a toy model representing the situation in Shu et al. (2006). In the broad sense, our work confirms that a process of magnetic field diffusion that does not rely on ambipolar diffusion is efficient.

Our setup assuming an axial gravitational field is a very simple model and ignores complications that could arise from using a spherical potential, like the tension of the magnetic field lines. The periodic boundary conditions give super-stability to the system, and do not allow inflow (or outflow) of material/magnetic field as we expect in a more realistic accretion process. However, our experiments can give us qualitative insights. They show that the turbulent diffusion of the magnetic field can remove magnetic flux from the central region, leading to a lower flux-to-mass ratio in regions of higher gravity compared with that of lower gravity.

We chose parameters to the simulations such that the system is not initially unstable to the Parker-Rayleigh-Taylor instability. Although the Parker instability could be present in real accretion systems and could help to remove magnetic field from the core of gravitational systems, its presence would make the interpretation of the results more difficult and we wanted to analyze only the turbulence role in the removal of magnetic flux. However, it is possible that this instability had been also acting due to local changes of parameters due to the turbulent motion. To ensure that the transport of magnetic flux is being caused by injection of turbulence only, we stopped the injection after a few time-steps in some experiments and left the system to evolve. When we did this, the changes in the profile of the magnetic field and the other quantities stopped.

We showed that the higher the strength of the gravitational force, the lower is the flux-to-mass ratio in the central region (compared with the mean value in the computational domain). This could be understood in terms of the potential energy of the system. When the potential is higher, more energetically favorable is the pile up of matter near the center of gravity, decreasing the total potential energy of the system. When the turbulence is increased, there is an initial trend to remove more magnetic flux from the center (and consequently more inflow of matter into the center), but for the highest value of the turbulent velocity in our experiments, there is a trend to remove material (together with magnetic flux) from the center, reducing the role of the gravity, due the fact that the gravitational energy became small compared to the kinetic energy of the system. Our results also showed

that when the gas is less magnetized (higher  $\beta$ , or higher values of the Alfvénic Mach number  $M_A$ ), the turbulent diffusion of magnetic flux is more effective, but the central flux-to-mass ratio relative to external regions is smaller for more magnetized models (low  $\beta$ ), compared to less magnetized models. That is, the contrast  $B/\rho$  between the inner and outer radius is higher for lower  $\beta$  (or  $M_A$ ).

If the turbulent diffusivity of magnetic field may explain the results in Shu et al. (2006), one may wonder whether one can remove magnetic field by this way not only from the class of systems studied by Shu et al. (2006), but also from less dense systems. For instance, it is frequently assumed that only ambipolar diffusion is important for the evolution of subcritical magnetized clouds (Tassis & Mouschovias 2005). Our study indicates that this conclusion may require modification in the presence of turbulence. This point, however, requires further careful study, which is beyond the scope of the present paper. In the future, we intend to study a more realistic model, e.g. with open boundary conditions and more realistic gravitational potentials.

## 8. TURBULENT MAGNETIC DIFFUSION AND TURBULENCE THEORY

Our study above reveals that in terms of heat transfer, the diffusion does not seem to be strongly affected by the presence of magnetic field. In terms of magnetic diffusion, magnetic configurations which hold up against gravity preserving the mass-to-flux ratio collapse to the lowest energy configurations concentrating mass and leaving out magnetic flux.

The key to understand these properties of magnetic field is related to the notion of magnetic turbulence being strong. In the picture of strong turbulence proposed by Goldreich & Sridhar (1995, henceforth GS95) the turbulence is being injected at the large scales with the injection velocity  $V_{inj}$  equal to the Alfvén velocity  $V_A$  (see Cho, Lazarian & Vishniac 2003 for a review). The turbulent eddies mix up magnetic field mostly in the direction perpendicular to the local magnetic field thus forming a Kolmogorov-type picture in terms of perpendicular motions. Naturally, these eddies are as efficient as hydrodynamic eddies in terms of heat advection. One can easily visualize how such eddies can induce magnetic field diffusion.

It is important to note that the GS95 model deals with motions with respect to the *local* rather than mean magnetic field. Indeed, it is natural that the motions of the parcel of fluid are affected only by the magnetic field of the parcel and of the near vicinity, i.e. by local fields. At the same time, in the reference frame of the mean field, the local magnetic fields of different parcels vary substantially. Thus we do not expect to see a substantial anisotropy of the heat advection when  $V_{inj} \sim V_A$ .

It was noted in LV99 that one can talk about turbulent eddies perpendicular to the magnetic field only if the magnetic field can reconnect fast. The rates of reconnection predicted in LV99 ensured that the magnetic field changes topology over one eddy turnover period. If the reconnection were slow, the magnetic fields would form progressively complex structures consisting of unresolved knots, which would invalidate the GS95 model. The response of such a fluid to mechanical perturbations would

be similar to “Jello”, making the turbulence-sponsored diffusion of magnetic field and heat impossible.

What happens when  $V_{inj} < V_A$ ? In this case the turbulence at large scales is weak and therefore magnetic field mixing is reduced. Thus one may expect a partial suppression of magnetic diffusivity. However, as turbulence cascades the strength of interactions increases and at a scale  $L_{inj}(V_{inj}/V_A)^2$  the turbulence gets strong. According to Lazarian (2006), the diffusivity in this regime decreases by the ratio of  $(V_{inj}/V_A)^3$ , with the eddies of strong turbulence playing a critical role in the process. When we compare the turbulent diffusivity  $\eta_{turb}$  estimated for the sub-Alfvénic models described in Table 3 (see §6) with  $L_{inj}V_{turb}(V_{turb}/V_A)^3$ , we find that the values are roughly consistent with the predictions of Lazarian (2006), although a more detailed study is required in this regard. For instance, we know that Lazarian (2006) theory was not intended for high Mach number turbulence.

All in all, we believe that the high diffusivity that we observe is related to the properties of strong magnetic turbulence. While the latter is still a theory which is subject to intensive study (see Boldyrev 2005, 2006; Lazarian & Beresnyak 2006; Beresnyak & Lazarian 2009a,b; Gogoberidze 2007), we believe that for the purpose of describing magnetic and heat diffusion the existing theory and the present model catch all the essential phenomena.

## 9. ACCOMPLISHMENTS AND LIMITATIONS OF THE PRESENT STUDY

### 9.1. Major findings

This paper presents several sets of simulations which deal with diffusion in magnetized turbulent fluids. The focus of the paper is on the diffusion of magnetic field, while the passive scalar, which may represent the diffusion of heat or metals in the media plays an auxiliary role. For example, we have presented comparisons of the diffusion of the passive scalar and the magnetic field and benchmarked our results against earlier studies.

Apparently, we see many similarities in the diffusion of heat and magnetic fields that is induced by turbulent motions. This result and its numerical testing would not make sense if the astrophysical reconnection were slow. Indeed, the major criticism that can be directed to the work of turbulent diffusion of heat by Cho et al. (2003) is that reconnection in their numerical simulations was fast due to high numerical diffusivity. With the confirmation of the LV99 model of turbulent reconnection by Kowal et al. (2009) one may claim that astrophysical reconnection is also generally fast and the differences between the computer simulations and astrophysical flows are not so dramatic as far as the reconnection is concerned.

In terms of heat transfer, we confirmed with higher resolution the results of Cho et al. (2003). In the subsequent sections, we extended the concept of efficient turbulent diffusion of heat for initially inhomogeneous distribution of magnetic field and in the presence of gravity.

The most important part of our study is the removal of magnetic fields from gravitationally bounded systems (see §6). Generally speaking, this is what one can expect on the energetic grounds. Magnetic field is a light fluid which is nearly not affected by gravity, while the mat-

ter tends to fall into the gravitational potential<sup>10</sup>. Turbulence in the presence of magnetic reconnection helps “shaking off” matter from magnetic fields. In our simulations the gravitational energy was larger than the turbulent energy. If the opposite is true, the system may get unbounded with turbulence mixing magnetic field in the same way it does in the absence of gravity (see §5).

It is important to note that in §6 we obtained the segregation of magnetic field and matter both in the case when we started with equilibrium distribution and in the case when the system was performing a free fall. In the case of non-equilibrium initial conditions the amount of flux removed from the forming dense core is substantially larger than in the case of the equilibrium magnetic field/density configurations (compare Figures 11 and 16). Nevertheless, the flux removal happens fast, essentially in one turnover of the turbulent eddies. In comparison, the effect of numerical diffusion for the flux removal in our simulations is marginal, and this is testified by the constant flux to mass ratio obtained in the simulations without turbulence (see Figure 16, right columns).

What is the physical picture corresponding to our findings? In the absence of gravity turbulence mixes up<sup>11</sup> flux tubes with different flux-to-mass ratios decreasing the difference in this ratio. In the presence of gravity, however, it is energetically advantageous of flux tubes at the center of the gravitational potential to increase the mass-to-flux ratio. This process is also facilitated by turbulence.

### 9.2. Applicability of the results

The application of the turbulent advection of heat is important for many astrophysical situations, e.g. to galaxy clusters. Our results indicate that an inhomogeneous distribution of magnetic field or/and the presence of gravitational potential does not suppress the process of heat advection.

The most interesting is, however, the diffusion of magnetic field. First of all, according to Figure 6 one may expect to see a broad distribution of magnetic field intensity with density. This seems to be consistent with the measurements of magnetic field strength in diffuse media (Troland & Heiles 1986).

The situation gets even more intriguing as we discuss magnetic field diffusion in the gravitational potential. It is tempting to apply these results to star formation process (see studies by Leão et al. 2009). There, clouds are known to be either magnetically supercritical or magnetically subcritical (see Mestel 1985). If, however, the magnetic flux can be removed from the gravitating turbulent cloud in a time scale of about an eddy turnover time, then the difference between clouds with different initial magnetization becomes marginal. The initially subcritical turbulent clouds can lose their magnetic flux via the turbulent diffusion to become supercritical.

An important point of the turbulent diffusion of the

<sup>10</sup> As a matter of fact, in our low  $\beta$  simulations, which we did not include in the paper, we also see signatures of the Parker instability.

<sup>11</sup> This mixing for Alfvénic modes happens mostly perpendicular to the local magnetic field for sub-Alfvénic and trans-Alfvénic turbulence (LV99). For super-Alfvénic turbulence the mixing is essentially hydrodynamic at large scales and the picture with motions perpendicular to the local magnetic field direction is restored at small scales.

magnetic field is that it does not require gas to be partially ionized, which is the requirement of the action of the ambipolar diffusion. Therefore, one may expect to observe gravitational collapse of the highly ionized gas. In fact, our present simulations are applicable to the fully ionized gas. The theory relating numerical simulations with rather high effective resistivity to the much better conducting astrophysical fluids is better justified for the fully ionized gases, as the corresponding model of reconnection, namely LV99 model, has been already numerically tested.

### 9.3. Magnetic field reconnection and different stages of star formation

Diffusion of magnetic field which is enabled by magnetic reconnection seems to be a fundamental process that accompanies all the stages of star formation.

In the turbulent scenario it is assumed that at the initial stages of star formation the concentration of material happens due to magnetic field moving along magnetic field lines (Vázquez-Semadeni et al. 2005). This one-dimensional process requires rather long times of accumulation of material.

Our work shows (§5) that 3D diffusion of magnetic field provides a wide distribution of the mass-to-flux ratios with some of the fluctuations having this ratio rather high. We believe that the diffusion of magnetic field described here is the reason for creation of zones of super-Alfvénic turbulence even for sub-Alfvénic driving (see Burkhart et al. 2009).

The regions of density concentration get gravitationally bound. One can associate such regions with GMCs. These entities are known to be highly turbulent and turbulent diffusion will proceed within them, providing a hierarchy of self-gravitating zones with different density and different mass-to-flux ratios. Some of those zones may be subcritical in terms of magnetic field and some of them may be supercritical. In subcritical magnetic cores the turbulent diffusion may proceed quasi-statically as we described in §6.2.1. and in the supercritical cores the turbulent diffusion may proceed as we described in §6.2.3. In both cases, we expect the removal of magnetic field from the self-gravitating cores. This process proceeds all the time, including the stage of the accretion disks.

What is the relative role of the ambipolar diffusion and the magnetic diffusion via reconnection<sup>12</sup>? This issue requires further studies. It is clear from the study by Shu et al. (2006) that in some situations the ambipolar diffusion is not fast enough to explain the removal of magnetic fields from accretion disks. This is the case when we claim that the magnetic diffusion through magnetic reconnection should dominate. Our study also shows that at the initial stages of concentration of gas the ambipolar diffusion is not necessary and, by itself, would provide unexceptionally long time scales for the process. At the same time, in cores with low turbulence, the ambipolar diffusion may dominate the reconnection diffusion. The exact range of the parameters for one or the other process

to dominate should be defined by future research.

### 9.4. Unsolved problems and future studies

Our paper has clearly exploratory character. For instance, to simplify the interpretation of our results we studied the concentration of material in the given gravitational potential, ignoring self-gravity of the gas. We plan to study this elsewhere.

In addition, our study indicates that the highly magnetized gas in gravitational potential is subject to instabilities (Parker-type) which drive turbulence and induce reconnection diffusion of magnetic field. This is another avenue that we intend to explore.

We report fast magnetic diffusion which happens at the rate of turbulent diffusion, but within the present set of simulations we do not attempt to precisely evaluate the rate. Thus we do not attempt to test, e.g., the predictions in Lazarian (2006) of the variations of the turbulent diffusion rate with the fluid magnetization for the passive scalar field. We also observe that while the magnetic field and the passive scalar field diffuse fast, there are differences in their diffusion arising, e.g. from magnetic field being associated with magnetic pressure. We have not attempted to quantify these differences in our work either.

The justification of our results being applicable to molecular clouds is based on the model of fast magnetic reconnection in the partially ionized gas in Lazarian et al. (2004). This model is the generalization of the LV99 model, but, unlike the LV99 model, it has not been numerically tested yet. Such testing may be very valuable in near future in view of our present study.

## 10. SUMMARY

Motivated by important astrophysical problems, such as the magnetic flux removal in star formation, the diffusion of heat and magnetic field in the interstellar and the intracluster media, in this paper we have studied the diffusion of magnetic field and a passive scalar that may represent heat, both in the absence and in the presence of gravitational potential. Recent work on validating the idea of reconnection supports our assertion that our results obtained at moderate resolution represent the dynamics of turbulent magnetic field lines in astrophysics. Our findings obtained on the basis of 3D MHD numerical simulations can be briefly summarized as follows:

1. Our results extend earlier findings of Cho et al. (2003) for heat advection by magnetized turbulence. We show that heat advection can be approximated by the product of the turbulence injection scale and the turbulent velocity for different Alfvénic and sonic Mach numbers.

2. In the absence of gravitational potential, we observe a clear difference in the diffusion of the passive scalar and the magnetic field, which arises from the dynamical effects of the magnetic field. The magnetic field diffuses removing strong anti-correlations of magnetic field and density that we impose at the start of our simulations. The system after several turbulent eddy turnover times relaxes to a state with no clear correlation between magnetic field and density, reminiscent of the observations of the diffuse ISM by Troland & Heiles (1986).

3. Our simulations that started with a quasi-static equilibrium in the presence of a gravitational potential,

<sup>12</sup> We feel that in analogy with ambipolar diffusion one can talk about turbulent “reconnection diffusion”. Unlike the Ohmic diffusion, which is slow on astrophysical scales, the reconnection diffusion can operate on the time scales of eddy turnovers.

revealed that the turbulent diffusivity allows gas to concentrate at the center of the gravitational potential, while the magnetic field is efficiently pushed to the periphery. Thus the effect of the magnetic flux removal from collapsing clouds and cores, which is usually attributed to ambipolar diffusion effect, can be successfully accomplished without ambipolar diffusion, but in the presence of turbulence.

4. Our simulations that started in a state of dynamical collapse induced by an external gravitational potential showed that in the absence of turbulence, the flux-to-mass ratio is preserved for the collapsing gas. On the other hand, in the presence of turbulence, a fast removal of magnetic field from the center of the gravitational potential occurs. This may explain the low magnetization observed in stars compared to the magnetization of the interstellar gas.

5. As an enhanced Ohmic resistivity to remove magnetic flux from cores and accretion disks has been ap-

pealed in the literature, e.g. by Shu et al. (2006), we have also compared models with a turbulent fluid and models without turbulence but with substantially enhanced Ohmic diffusivity. We have shown that, in terms of the magnetic flux removal, the turbulent diffusivity can sometimes mimic the effect of an enhanced Ohmic resistivity.

RSL and EMGDP acknowledge partial support from grants of the Brazilian Agencies FAPESP (2006/50654-3 and 2007/04551-0), CAPES (PDEE 3979-08-3) and CNPq. RSL is also grateful to the members and staff of the Astronomy Department of the University of Wisconsin for their hospitality during his visit there. AL acknowledges the NSF grant AST 0808118 and the NSF-sponsored Center for Magnetic Self-Organization. JC was supported in part by Korea Research Foundation (KRF-2006-331-C00136).

#### REFERENCES

- Beresnyak, A., & Lazarian, A. 2009a, *ApJ*, 702, 1190  
 Beresnyak, A., & Lazarian, A. 2009b, *ApJ*, 702, 460  
 Biskamp, D. 1986, *Physics of Fluids*, 29, 1520  
 Boldyrev, S. 2005, *ApJ*, 626, L37  
 Boldyrev, S. 2006, *Physical Review Letters*, 96, 115002  
 Burkhart, B., Falceta-Gonçalves, D., Kowal, G., & Lazarian, A. 2009, *ApJ*, 693, 250  
 Cho, J., Lazarian, A., Honein, A., Knaepen, B., Kassinos, S., & Moin, P. 2003, *ApJ*, 589, L77  
 Cho, J., Lazarian, A., & Vishniac, E. T. 2003, *ApJ*, 595, 812  
 Dobrowolny, M., Mangeney, A., & Veltri, P. 1980, *Physical Review Letters*, 45, 144  
 Draine, B. T., & Lazarian, A. 1998, *ApJ*, 508, 157  
 Elmegreen, B. G., & Scalo, J. 2004, *ARA&A*, 42, 211  
 Esquivel, A., Benjamin, R. A., Lazarian, A., Cho, J., & Leitner, S. N. 2006, *ApJ*, 648, 1043  
 Falceta-Gonçalves, D., Lazarian, A., & Kowal, G. 2008, *ApJ*, 679, 537  
 Galli, D., Lizano, S., Shu, F. H., & Allen, A. 2006, *ApJ*, 647, 374  
 Giacalone, J., & Jokipii, J. R. 1999, *ApJ*, 520, 204  
 Gogoberidze, G. 2007, *Physics of Plasmas*, 14, 022304  
 Goldreich, P., & Sridhar, S. 1995, *ApJ*, 438, 763  
 Heitsch, F., Zweibel, E. G., Slyz, A. D., & Devriendt, J. E. G. 2004, *ApJ*, 603, 165  
 Higdon, J. C. 1984, *ApJ*, 285, 109  
 Iroshnikov, P. S. 1963, *AZh*, 40, 742  
 Kowal, G., Lazarian, A., & Beresnyak, A. 2007, *ApJ*, 658, 423  
 Kowal, G., Lazarian, A., Vishniac, E. T., & Otmianowska-Mazur, K. 2009, *ApJ*, 700, 63  
 Kraichnan, R. H. 1965, *Physics of Fluids*, 8, 1385  
 Kulpa-Dybel, K., Kowal, G., Otmianowska-Mazur, K., Lazarian, A., & Vishniac, E. 2009, arXiv:0909.1265  
 Lazarian, A. 2006, *ApJ*, 645, L25  
 Lazarian, A., & Beresnyak, A. 2006, *MNRAS*, 373, 1195  
 Lazarian, A., & Vishniac, E. T. 1999, *ApJ*, 517, 700  
 Lazarian, A., Vishniac, E. T., & Cho, J. 2004, *ApJ*, 603, 180  
 Leão, M. R. M., de Gouveia Dal Pino, E. M., Falceta-Gonçalves, D., Melioli, C., & Geraissate, F. G. 2009, *MNRAS*, 394, 157  
 Lesieur, M. 1990, NASA STI/Recon Technical Report A, 91, 24106  
 McKee, C. F., & Ostriker, E. C. 2007, *ARA&A*, 45, 565  
 Mestel, L. 1985, *Physica Scripta Volume T*, 11, 53  
 Montgomery, D., & Turner, L. 1981, *Physics of Fluids*, 24, 825  
 Padoan, P., Jimenez, R., Juvella, M., & Nordlund, Å. 2004, *ApJ*, 604, L49  
 Parker, E. N. 1958, *ApJ*, 128, 664  
 Petschek, H. E. 1964, NASA Special Publication, 50, 425  
 Richardson, L. F. 1926, Royal Society of London Proceedings Series A, 110, 709  
 Shay, M. A., Drake, J. F., Denton, R. E., & Biskamp, D. 1998, *J. Geophys. Res.*, 103, 9165  
 Shay, M. A., Drake, J. F., Swisdak, M., & Rogers, B. N. 2004, *Physics of Plasmas*, 11, 2199  
 Shebalin, J. V., Matthaeus, W. H., & Montgomery, D. 1983, *Journal of Plasma Physics*, 29, 525  
 Shu, F. H. 1983, *ApJ*, 273, 202  
 Shu, F. H., Galli, D., Lizano, S., & Cai, M. 2006, *ApJ*, 647, 382  
 Sweet, P. A. 1958, *Electromagnetic Phenomena in Cosmical Physics*, 6, 123  
 Tassis, K., & Mouschovias, T. C. 2005, *ApJ*, 618, 769  
 Troland, T. H., & Heiles, C. 1986, *ApJ*, 301, 339  
 Uzdensky, D. A., & Kulsrud, R. M. 2000, *Physics of Plasmas*, 7, 4018  
 Vázquez-Semadeni, E., Kim, J., Shadmehri, M., & Ballesteros-Paredes, J. 2005, *ApJ*, 618, 344  
 Yamada, M., Ren, Y., Ji, H., Breslau, J., Gerhardt, S., Kulsrud, R., & Kuritsyn, A. 2006, *Physics of Plasmas*, 13, 052119